CLNS 317
August 1975

Inclusive and Exclusive Virtual Photoproduction Results from Cornell

Kenneth M. Hanson*

Laboratory of Nuclear Studies
Cornell University
Ithaca, New York 14853

A talk given at the 7th International Symposium on
Lepton and Photon Interactions at High Energies
August 21-27, 1975
Stanford University

*Work supported by the National Science Foundation

1. Introduction

The property of scaling in inclusive electron-nucleon scattering discovered by the SLAC-MIT collaboration quickly led to the acceptance of the notion that the nucleons are composed of point-like objects called partons[1]. In an attempt to learn more about the elementary processes taking place in deep-inelastic electron scattering, a large number of electroproduction experiments have been undertaken in which one or more of the final state hadrons were observed. In this report I would like to describe the results from a series of electroproduction experiments performed during the last several years at the Wilson Synchrotron Laboratory of Cornell University in which the scattered electron and a single charged hadron are detected in the final state. Professor Frank Pipkin and his group from Harvard University have been involved in this whole series of experiments on a continuing basis. A group of us from Cornell became involved only in the last round of experiments. The participants from Harvard were Chris Bebek, Chuck Brown, Phil Bucksbaum, Martin Herzlinger, Steve Holmes, Bob Kline, Carl Lichtenstein, Frank Pipkin, Siegbert Raither, and Keith Sisterson. Those from Cornell included Andy Browman, Dave Larson, Al Silverman, and myself.

When one is trying to characterize the final hadronic state of an electroproduction process, it is convenient to think in terms of the corresponding virtual photoproduction process as shown in Fig. 1. The scattering of the electron from the hadronic side of the diagram is mediated by a virtual photon. From the knowledge of the incident and final electron momenta, one can define the mass, $-Q^2$, energy, ν, and direction of the virtual photon. In our experiments, then, we regard the incident electron beam and the detected final electron as defining a beam of virtual photons with flux Γ. The transverse and longitudinal polarization state

of the virtual photons is given by the parameter ε.

The apparatus used in the experiments I am describing consist basically of two spectrometers: one to detect the scattered electron and the other to detect an outgoing charged hadron. The momentum resolution of the spectrometers is typically on the order of 1%. The electron is identified by means of a Cherenkov and shower counter. The hadron identification is accomplished through a combination of a time-of-flight measurement and a Cherenkov counter. It should be noted that the use of such a spectrometer system allows us to cleanly identify the process under consideration both in terms of particle identification and in terms of the kinematical quantities.

With the two spectrometer system used, it is possible to study the following virtual photoproduction processes

$$\gamma_v + N \rightarrow \pi^{\pm} + x$$

$$\gamma_v + N \rightarrow K^{+} + x$$

$$\gamma_v + N \rightarrow p + x$$

When the measured cross sections are plotted versus the missing mass squared, M_x^2, a limited number of exclusive two-body final states are observed in all of the above reactions. The bulk of the data, however, cannot be so identified and is treated in terms of inclusive reactions. The data are analyzed in terms of the invariant structure function

$$F = \frac{E_h}{\sigma_{tot}} \frac{d\sigma}{d^3 p_h} = \frac{E^*}{\sigma_{tot} \pi p^*_{max}} \frac{d\sigma}{dx\, dp_\perp^2} \tag{1}$$

$$= \frac{1}{\sigma_{tot}} \frac{E^*}{\pi [p^*_{max}{}^2 - p_\perp^2]^{1/2}} \frac{d\sigma}{dx' dp_\perp^2} \tag{2}$$

Here x and x' are defined as

$$x = p^*_{//} / p^*_{max} \tag{3}$$

$$x' = p^*_{//} / (p^{*2}_{max} - p^2_{\perp})^{1/2} \tag{4}$$

where $p^*_{//}$ ($p_{\perp}$) is the component of the detected hadron's momentum parallel (perpendicular) to the virtual photon direction in the center of mass (CM) of the final hadronic system (which is the same as the virtual photon-proton CM) and p^*_{max} is the hadron's maximum possible CM momentum. σ_{tot}, the total virtual photoproduction cross section, is divided out to remove the gross Q^2 and W dependence of the cross sections. This allows us to concentrate on changes in the form of invariant cross section that might exhibit themselves as a function of Q^2 and W.

Fig. 2 schematically shows the regions in CM phase space covered by our recent experiments. $x_{\perp}$ is defined as

$$x_{\perp} = p_{\perp} / P^*_{max} \tag{5}$$

The data obtained in previous two-spectrometer experiments have principally been restricted to region A (along virtual photon direction) and furthermore have been restricted to Q^2 less than 2 GeV^2 and ε close to 1. Data now have been obtained in region A up to Q^2 = 4 GeV^2. Our most recent experiments have pushed the measurements to the kinematic limit in $p_{\perp}$ in the "central" region for pions and in the backward hemisphere for protons (region B).

In this report I will discuss the reactions observed taking each particle type in turn. I will make comparisons between regions A and B as I go along. I will also make a few comments about some calculations we have made concerning the radiative corrections to inclusive cross sections.

2. Exclusive Pion Reactions

When a single pion is observed, the dominant exclusive reaction is the one with a pion and a nucleon in the final state. In this discussion I will confine myself to this reaction.

2.1 Forward Direction

In the forward direction, new data have been taken by the Harvard group for the following reactions:

$$\gamma_v + p \to \pi^+ + n$$
$$\gamma_v + d \to \pi^+ + n + n_s$$
$$\gamma_v + d \to \pi^- + p + p_s$$

The first reaction had been studied extensively[2-6] up to $Q^2 = 2$ GeV^2. The measured cross sections have been well accounted for by dispersion theory calculations, for example that done by Berend's[7]. The dominance of the cross section by the pion pole term has been used to determine the pion form factor, F_π. Berend's makes the assumptions that 1) The amplitude is imaginary only in the resonance region, and 2) the only multipole contribution is from the M_1^+ of the $\Delta(1236)$. The calculation uses the generalized Born approximation for the single nucleon and pion poles. One deficiency of this calculation is that there is no allowance for a possible isoscalar contribution to the amplitude. Measurements now have been made using a D_2 target which allow the determination of the isoscalar contribution through the ratio

$$R = \frac{\sigma(\gamma_v + d \to \pi^- + p + p_s)}{\sigma(\gamma_v + d \to \pi^+ + n + n_s)} = \frac{|A_v|^2 + |A_s|^2 - 2\,\mathrm{Re}\, A_s^* A_v}{|A_v|^2 + |A_s|^2 + 2\,\mathrm{Re}\, A_s^* A_v} \qquad (6)$$

where A_s and A_v are the isoscalar and isovector amplitudes. The new experiments also extend the measurements of the pion form factor up to Q^2=4 GeV^2.

Fig. 3 shows the measured missing mass squared spectra obtained on both H_2 and D_2. The above reactions can be cleanly identified. In Fig. 4 the ratio R for several different Q^2 and W values is plotted against t, the square of the four momentum transfer to the nucleon. The lowest Q^2 data come from earlier CEA experiments. R appears to be a universal function of t. The form

$$1 - A\sqrt{-t} \tag{7}$$

fits the data quite well with a value for A of 0.817 ± 0.058 GeV^{-1}. Photoproduction measurements[8-12] show a similar dependence on t but with a somewhat larger value for A. The major part of the isoscalar contribution to the H_2 cross sections can be removed by multiplying them by $\frac{1}{2}(1 + R)$. The resulting cross sections are radiatively corrected[13] and analyzed using Berend's theory to obtain F_π. If this procedure is correct, the value of F_π obtained at fixed Q^2 should be independent of W. Fig. 5 demonstrates this, where the dependence upon W is represented in terms of the minimum momentum transfer. The Q^2 dependence of F_π is shown in Fig. 6 both with and without the correction for the isoscalar contribution. The effect on F_π of subtracting the isoscalar contribution is less than 10% for all but the highest Q^2 data point. With the isoscalar subtraction, the data tend to favor F_1^V, the Dirac isovector form factor of the nucleon, over the rho form factor, F_ρ, particularly at low Q^2. A fit of the form

$$F_\pi = (1 + Q^2/M_V^2)^{-1} \tag{8}$$

gives a χ^2 of 20.4 for 16 degrees of freedom with $M_V^2 = 0.471 \pm 0.010$ GeV^2.

2.2 Large CM Angles

The parton interchange model of Brodsky and Farrar[14] prompted us to investigate the reaction

$$\gamma_v + p \rightarrow \pi^+ + n$$

at large momentum transfers. This model predicts for any reaction a + b → c + d an s (total CM energy squared) dependence of the cross section for a fixed CM angle:

$$\frac{d\sigma}{dt} = \frac{f(\theta^*)}{s^{N-2}} \qquad (9)$$

when s and t are large. N is the total number of elementary fields contained in the initial and final states. This model has met with good success in a variety of reactions when quarks are counted as the elementary fields of the hadrons[15]. In particular, in the above reaction the model predicts an S^{-7} dependence. This has been verified in photoproduction[16] where the exponent is measured to be 7.3 ± 0.4.

Our data cover the following kinematic ranges: $1.2<Q^2<4.4$ GeV^2, $1.2<W<3.0$ GeV, $55°<\theta^*<95°$. Fig. 7 shows the CM angular distribution of the measured cross sections at W = 2.65 GeV. The cross sections have been radiatively corrected using the formalism of Bartl and Urban[13]. The cross sections are observed to drop three orders of magnitude in going from the forward direction to 90°. The W variation of the cross sections are shown in Fig. 8 for several different CM angles at Q^2 = 1.2 GeV^2. It is found that the data above W = 2.0 GeV are fit well by the form

$$\frac{d\sigma}{d\Omega^*} = \frac{a_1}{(Q^2)^{a2}\, W^{a3}} \qquad (10)$$

The values of a_3 obtained for the four CM angles, θ^* = 60°, 70°, 80°, 90° are 7.5±1.1, 10.4±0.7, 11.6±0.5, 12.9±0.7, respectively. These fits are displayed in Fig. 8. The W dependence becomes weaker as θ^* decreases, which

it must, since in the forward direction, $\frac{d\sigma}{d\Omega^*}$ falls off roughly as W^{-2}. The parton interchange model prediction, when transcribed into the above representation of the cross section is that a_3 should be 12. This is in agreement with our results at $\theta^* = 80°$ and 90°. Our result is consistent with the photoproduction measurements ($a_3 = 12.6 \pm 0.8$, in our notation). Furthermore, we see no observable dependence of a_3 upon Q^2 within our data set. Thus, Q^2 seems to have no effect upon the s (or W) dependence of the cross section for this reaction.

Fig. 9 shows the Q^2 dependence of $\frac{d\sigma}{d\Omega^*}$ for two W regions. We notice there is very little change as Q^2 goes between 0 and 1 GeV^2. But above $Q^2 = 1$ there is a rapid falloff of the cross section, perhaps as fast as $(Q^2)^{-2}$. There is a striking similarity between the Q^2 variation at large θ^* and that in the forward direction. In the forward direction the initial rise with Q^2 is due to an increasing longitudinal contribution from the one pion exchange diagram. One wonders whether this similarity means there is a large longitudinal contribution to the cross section at 90°. This would be contrary to the simple quark model prediction that only transverse photons contribute. The simple quark model suggests that the dominant processes at $\theta^* = 90°$ is the interaction of the virtual photon with a single quark. Since the quarks are thought to be point-like, this would imply a slow Q^2 dependence of the cross sections at 90°, in contrast with the rather rapid variation we observe above $Q^2 = 1$ GeV^2.

3. Inclusive Reactions

3.1 Forward Direction

The forward direction is the virtual photon fragmentation region. Naively, it is here that we would expect to first observe a dependence upon the virtual photon's characteristics, Q^2 and ν. To understand the inclusive virtual photoproduction of pions in terms of the quark-parton model, Feynman [18] and Gronau, Ravndal and Zarmi [19] assume that the process can be broken up into two independent steps - 1) ejection of a single quark by the virtual photon, and 2) the fragmentation of the quark into hadrons. It is further assumed that the fragmentation processes of the ejected quark and the left-over quarks are independent. The inclusive cross sections are then given by a sum over all possible quark contributions of the product of a parton distribution function times a parton fragmentation function, e.g., $u(\omega)\ D_u^+(x)$, where ω is the scaling variable $\frac{2M\nu}{Q^2}$, and x is $P_{//}^*/P_{max}^*$. As a minimum consequence of this factorization, at a fixed value of x, the inclusive cross sections should scale with ω. Much of this section will be devoted to the question of whether the data show such a scaling with ω.

Pipkin's group from Harvard has made measurements at the Cornell synchrotron which thoroughly explore the forward region over a range of $0.6<Q^2<3.9$ GeV^2, and $2.2< W< 3.1$ GeV. Measurements were made on both H_2 and D_2. Fig. 10 shows the invariant structure functions measured on H_2 for both π^+ and π^-. Since it is difficult to see any but the most gross feature of the data from plots such as this, the procedure is adopted of taking the ratio of the measured cross sections to a common function. The function used for data which have not been radiatively connected is

$$f = \exp\,(0.656 - 3.26\,x' - 3.00\,x'^2 + 4.35\,x'^3) \qquad (11)$$

where the coefficients are determined by fitting to the data at W= 3.1 GeV (both Q^2 values). When radiative corrections are made to the data (see Section 4) the function used is

$$f = \exp (0.555 - 1.85\ x' - 5.98\ x'^2 + 6.26\ x'^3) \qquad (12)$$

Figure 11 shows the results of applying this procedure to the π^+ data from proton. Figure 12 shows the corresponding results for both π^+ and π^- data from neutrons (as deduced from a subtraction of the H_2 data from the D_2 data). One sees in these graphs anomalous contributions at large x' particularly at small W or small Q^2 arising from the $\pi\ \Delta$ final states. Aside from these effects, the distributions have a discernable dependence on W but apparently no variation with Q^2. That is to say, the invariant structure function for π's does not seem to scale with ω!

Dakin and Feldman have shown [20] the parton model predicts a strong dependence on ω of the $\pi^+/\ \pi^-$ ratio in the forward direction. This ratio is relatively free of normalization uncertainties and thus might be thought to be directly comparable from experiment to experiment. Unfortunately, many previous experiments did not distinguish between π^+ and K^+ and p. This has a sizeable effect on $\pi^+/\ \pi^-$ (about 30-40%). The new data [21] improve on the statistical accuracy of the π^+/π^- ratios using cleanly identified pion samples. Figs. 13 and 14 show the x' dependence of the π^+/π^- ratio for proton and neutron targets. There is very little structure visible in the region $x' < 0.7$. There is no observable dependence of π^+/π^- upon $p_\perp^2$, as demonstrated for the proton target data in interval, $0.5 < x' < 0.7$ in Fig. 15. In order to look at the overall Q^2 and/or W dependence of these data, the data up to $p_\perp^2 = 0.2\ GeV^2$ have been combined for x' less than 0.7 (to avoid $\pi\ \Delta$ region) and x' greater than 0.3 (to avoid "central" region). Fig. 16 shows the results plotted separately

against $1/\omega$ and against W. As has been the case in the past, these data still do not allow one to unequivically choose between the two possibilities 1) π^+/π^- is a function only of ω, i.e., scales in ω or 2) π^+/π^- is a function only of W. The variation of π^+/π^- with W or $1/\omega$ is just too small over the measured range of the parameters to see a significant difference between these two choices.

The invariant structure functions for protons produced close to the $\vec{q}$ direction are shown in Fig. 17 for a few of the (Q^2, W) points [22]. One observes very little Q^2 dependence at fixed x'. In the forward direction (x'>0), however, the number of protons drops off rapidly as W increases. The distributions clearly do not scale with ω. An interesting feature of the data seen in Fig. 17 is that the number of protons produced in the forward direction is roughly the same for a neutron target as for a proton target. More quantatively, the ratios of the number of protons from a neutron target to that for a proton target in the region $0.1 < x' < 1.0$ and $p_\perp^2 < 0.02$ GeV^2 for (Q^2, W) values of (1.2 GeV^2, 3.1 GeV), (1.2, 2.2) and (4.0, 2.2) are 0.82 ± 0.19, 0.85 ± 0.13 and 0.82 ± 0.44, respectively.

The measurement of the inclusive spectra for kaons is experimentally somewhat more difficult than for pions or protons owing to their relative infrequency and the substantial corrections for their decay before reaching the end of the spectrometer. The invariant structure functions for K^+ mesons obtained at a variety of (Q^2, W) points are shown in Fig. 18. The irregularities seen above $x' = 0.6$ are due to the exclusive reactions in which X is a Λ, Λ' or Σ. For $x' < 0.6$ the K^+ data show little variation with Q^2 or W (within the rather large error bars). Comparison of the data with the line drawn in Fig. 18 shows that the invariant structure function for K^+ is roughly 20% of that for π^+.

3.2 Central (or Backward) Region

The success of the parton interchange model in describing the W dependence of our exclusive $\pi^+ n$ cross sections at $\theta^* = 90^0$ leads us to try it for our inclusive reaction results. The parton interchange model of Blankenbecler, Brodsky, and Gunion [23] predicts that, for large s and large t, the inclusive invariant cross section should scale according to

$$E \frac{d\sigma}{d^3p} = \frac{1}{s^{N-2}} f\left(\frac{t}{s}, \frac{M_x^2}{s}\right) \qquad (13)$$

where N is the number of constituent fields participating in the specific inclusive reaction. Note that t/s is simply a function of θ^*. At $x = 0$ ($\theta^* = 90^0$), this becomes

$$\frac{E}{\sigma_{tot}} \frac{d\sigma}{d^3p} = F = \frac{1}{W^n} f(x_\perp) \qquad (14)$$

($W = \sqrt{s}$)[24]. This type of scaling has been observed at the FNAL and the ISR [25] for inclusive pion distributions resulting from p-p interactions at high energies. For $x > 0.4$ and $W > 19$ GeV, n is found to be independent of $x_\perp$.

Inclusive pion virtual photoproduction data near $x = 0$ have been obtained in the most recent Harvard-Cornell measurements. Fig. 19 shows the π^+ invariant structure functions displayed as a function of $x_\perp$. The curves drawn in Fig. 19 represent a fit to the data which has no Q^2 dependence. By comparing the data with the curves, one observes that the data possess no dependence upon Q^2. There is, however, a substantial dependence upon W. We have made a fit to the data of the form given by eq. 14. n, the exponent of W, is found to be a function of $x_\perp$ as shown in Fig. 20. This is contrary to the parton interchange model prediction that n should be independent of $x_\perp$. The straight line drawn in Fig. 20 is the result of a fit to the data with the parameterization:

$$n = (13.4 \pm 0.4)\ x_\perp^{(1.71 \pm 0.05)}.$$

It is interesting to note that when the W dependence for the $\pi^+ n$ exclusive reaction at $\theta^* = 90^o$ (Sec. 2.2) is converted to the form of the structure function, it is found to behave as $W^{-13.9 \pm 0.7}$, whereas the interpretation of the inclusive reaction result to $x_\perp = 1$ gives $W^{-13.4 \pm 0.4}$. Thus the exclusive reaction appears to represent a continuous extension of the inclusive reaction (or visa versa!).

In the search for a simpler representation of the W dependence of the inclusive π^+ data, we found the cross sections $\frac{d\sigma}{d\Omega^* dM_X^2}$ when plotted versus M_X^2 display a type of scaling as shown in Fig. 21. The curves drawn represent a fit to the cross sections of the form $W^{-n} f(M_X^2)$. It is interesting to note that our data below $Q^2 = 2.4$ GeV^2 give a value $n = 12.6 \pm 0.3$ which is consistent with the exclusive $\pi^+ n$ reaction result of 12.9 ± 0.7. This means that $\frac{d\sigma}{d\Omega^* dM_X^2}$ has the same W^{-n} dependence for all M_X irrespective of whether the contributing reactions are inclusive or exclusive.

Another way of presenting the inclusive π^+ results is to plot the invariant structure function as a function of $p_\perp^2$, as in Fig. 22. When plotted this way, it is seen that the data show a much slower dependence upon W then when plotted versus $x_\perp$. The π^+ structure function behaves as $e^{-bp_\perp^2}$ but with a break in slope occurring around $p_\perp^2 = 0.15$ GeV^2. The value of b found for $p_\perp^2 < 0.15$ GeV^2 is about 10 GeV^{-2} throughout the range covered: $2.2 < \omega < 3.2$ GeV, $1.2 < Q^2 < 3.6$ GeV^2. The value of b for $p_\perp^2 > 0.15$ GeV^2 is about 6 GeV^{-2}, with only a slight W dependence observed.

Fig. 23 demonstrates the lack of a Q^2 dependence of the π^- structure function in the central region when W is fixed. Our measurements at $Q^2 = 1.2$ GeV^2 agree very well with the S-B-T collaboration photoproduction results [26]!

The π^+/π^- ratio near x= 0 is plotted in Fig. 24 as a function of $x_\perp$ for a number of (Q^2, W) points. The data show no $x_\perp$ dependence. The ratios integrated over all $x_\perp$ are shown in Fig. 24 separately as a function of $1/\omega$ and W. It is clear that in the central region the π^+/π^- ratios do not scale with ω. They seem to be a function only of W, however. When the π^+/π^- ratios plotted versus W are compared with the same ratios obtained in the forward direction, Fig. 16, one observes that the $\theta^*= 0^o$ and $\theta^*= 90^o$ results are very similar with the exception of the $Q^2= 1.2$ GeV^2, W= 2.2 GeV forward point. This suggests that for large Q^2 and W the π^+/π^- ratio is isotropic, that is, independent of both $x_\perp$ and x.

The proton data obtained simultaneously with central region pion data, lie in the backward hemisphere in the CM (region B of Fig. 2). This is the target fragmentation region and the expectation is that as x approaches -1 the inclusive cross sections should become independent of the (photon) projectile's characteristics. The interpretation of the measured cross sections in terms of inclusive reactions becomes complicated by the presence of a number of exclusive reactions as shown in Fig. 26. One observes mass peaks for the forward production of the π^o, η^o and ρ^o. When we want to exclude these processes in the present discussion we will simply exclude the region $M_X^2 < 0.75$ GeV^2.

Fig. 27 shows the proton invariant structure function plotted as a function of $x_\perp$ for an x interval roughly in the middle of the experimental acceptance. To guide the eye the same curves are drawn for each Q^2 interval. It is seen that the data show only a modest dependence upon Q^2. In order to describe the W dependence we have parametrized the cross sections in a manner similar to the inclusive pion data, namely according to eq. 14. The value of n obtained by

fitting the data to this form is a function of $x_\perp$ quite similar to that obtained for the pion data at $x = 0$. The fit to the data above $x_\perp = 0.35$ for $M_X^2 > 0.75$ GeV^2 shown in the figure has the parametrization $n = (14.6 \pm 0.8)\, x_\perp^{(2.06 \pm 0.1)}$. It is interesting that the intercept at $x_\perp = 1$ is consistent with being the same as for the inclusive pion data. The exclusive reaction at this kinematic limit is $\gamma_v + p \rightarrow \pi^o + p$ which, according to the parton interchange model, should have the same W dependence as the $\gamma_v + p \rightarrow \pi^+ + n$.

The proton invariant structure function is plotted versus $p_\perp^2$ in Fig. 29. The structure function has a much weaker dependence upon W when presented in this way. In particular, for $p_\perp^2 < 0.5$ GeV^2 the data show essentially no W dependence. For larger $p_\perp^2$ the results from the largest two W intervals tend to be closely similar although they are decidedly different. When the data with $M_X^2 > 0.75$ GeV^2 are fit to a form $e^{-bp_\perp^2}$, the values of b obtained are about 4.0, independent of both Q^2 and W.

We have looked in a preliminary fashion for K^+ mesons in this same data sample. So far we have not seen any. At present the upper we can place on K^+ production near $X = 0$ for $Q^2 = 1.2$ GeV^2 is $\frac{K^+}{\pi^+} < 0.1$.

4. Radiative Corrections to Inclusive Cross Sections

In the past, radiative corrections have not normally been applied to inclusive virtual photoproduction cross sections principally because these corrections are not easy to calculate and it was felt that the corrections would not be very significant anyway. The experimental geometry used in the measurement of the cross sections at large θ^* reported in Section 3 was such that it led to the possibility of a significant contribution arising from hadrons produced at small θ^* in radiative events. We developed a technique for calculating the

radiative corrections to inclusive cross sections to answer the question of how significant these corrections are.

The three major ingredients in the calculation are

1. Equivalent radiator method
2. Peaking approximation
3. Assumed virtual photoproduction cross sections.

The equivalent radiator method was taken from Mo and Tsai [27]. It allows one to separate the radiative processes into those events in which a hard photon is radiated before the electron scatters and those in which the photon is radiated after scattering. The peaking approximation here refers to the assumption that the photon is emitted along the radiating electron direction. This allows one to easily calculate the properties of the virtual photon (ν, Q^2, direction) in the scattering process. It has been assumed that the virtual photoproduction invariant structure function can be adequately represented as a simple function of x' and $p_\perp$ which has no Q^2 or W dependence. It has been found that the calculated radiative corrections do not depend significantly on the details of the function used. The present calculations ignore radiation by the hadrons and may well have a systematic uncertainty as large as 10%.

The results of our calculations are shown in Fig. 30 and 31 for pions in the forward and central regions. It is observed that the radiative corrections are small (about 10%) in our (Q^2, W) range except near the kinematic boundaries. The radiative corrections at different (Q^2, W) points have essentially the same x' or $x_\perp$ dependence. Hence between different (Q^2, W) points the basic effect of the corrections is to change the overall normalizations. Most of the cross sections presented in this report do not include radiative corrections partly because the radiative correction calculations have been completed only recently

and partly because their effect is not much larger than the systematic uncertainties in the measurements. In total, the radiative corrections do not change the conclusions made on the basis of the data without the corrections.

5. Conclusion

The cross section for the virtual photoproduction of the $\pi^+ n$ final state where the π^+ is produced along the $\vec{q}$ direction is found to contain a significant contribution from the isoscalar amplitude. When the cross sections are corrected for this isoscalar contribution, F_π is reduced slightly and roughly follows F_1^V. The inclusive reactions in the forward direction do not appear to scale with ω, as predicted by the parton model, but tend to scale with W. The values of W for which the measurements were taken, $2.2 < W < 3.2$ GeV, may be too low for the assumptions made about parton fragmentation to hold. Near $\theta^*=90°$ it is found that for the $\pi^+ n$ exclusive virtual photoproduction reaction $\frac{d\sigma}{d\Omega^*}$ behaves as $W^{-12.9\pm0.7}$ down to an astonishing low value of W of 1.7 GeV in agreement with the prediction of the parton interchange model. However, the Q^2 dependence of the cross section is hard to understand within the context of this model. The inclusive cross sections near $x=0$ ($\theta^*=90°$) also scale as W^n at fixed $x_\perp$ but n is not independent of $x_\perp$ as the parton interchange model suggests. Again, W may be too low for this model to be valid here. Radiative corrections to the inclusive cross sections are small and do not alter significantly the conclusions drawn from the measurements.

Acknowledgements

I would like to thank the members of the Harvard and Cornell groups listed in the Introduction without whose efforts this talk would not have been possible. I am grateful to Terry Schalk and William Tannenbaum for their assistance.

References

1. W. K. H. Panofsky, Proc. 14th International Conf. on High Energy Physics, Vienna, 1968. For recent summary, see E. D. Bloom, Proc. 6th International Symposium on Electron and Photon Interactions at High Energies, Bonn (1973), North Holland, Amsterdam, 1974.
2. For a brief summary of the theory and a more complete set of references, see C. N. Brown, C. R. Canizares, W. E. Cooper, A. M. Eisner, G. J. Feldman, C. A. Lichtenstein, L. Litt, W. Lockeretz, V. B. Montana, and F. M. Pipkin, Phys. Rev. D8, 92 (1973).
3. C. J. Bebek, C. N. Brown, M. Herzlinger, S. Holmes, C. A. Lichtenstein, F. M. Pipkin, L. K. Sisterson, D. Andrews, K. Berkelman, D. G. Cassel, and D. L. Hartill, Phys. Rev. D9, 1229 (1974).
4. C. Driver, K. Heinloth, K. Höhne, G. Hofmann, P. Karow, A. Schmidt, G. Specht, and J. Rathje, Phys. Lett. 75B, 77 (1971).
5. P. S. Kummer, A. B. Clegg, F. Foster, G. Hughes, R. Siddle, J. Allison, B. Dichinson, E. Evangelides, M. Ibbotson, R. Lawson, R. S. Meaburn, H. E. Montgomery, W. J. Shuttleworth and A. Sofair, Nuovo Cimento Lett. 1, 1026 (1971).
6. A. Sofair, J. Allison, B. Dickinson, E. Evangelides, M. Ibbotson, R. Lawson, R. S. Meaburn, H. E. Montgomery, W. J. Shuttleworth, A. B. Clegg, F. Foster, G. Hughes, P. Kummer, and R. Siddle, Nucl. Phys. B42, 369 (1973).
7. F. A. Behrends, Phys. Rev. D1, 2590 (1970).
8. P. Heide, U. Kötz, R. A. Lewis, P. Schmüser, H. S. Skronn, and H. Wahl, Phys. Rev. Lett, 21, 248 (1967).
9. A. M. Boyarski, R. Diebold, S. D. Ecklund, G. F. Fischer, Y. Murata, B. Richter, and W. S. C. Williams, Phys. Rev. Lett. 21, 1767 (1968).
10. Z. Bar-Yam, J. de Pagter, M. M. Hornig, W. Kern, D. Luckey, and L. S. Osborne, Phys. Rev. Lett.19, 40 (1967).

11. R. Worden, Nucl. Phys. B37, 253 (1972).

12. G. Goldstein and J. F. Owens III. (to be published).

13. A. Bartl and P. Urban, Acta. Phys. Austriaca 24, 139 (1966).

14. S. J. Brodsky and G. R. Farrar, Phys. Rev. Lett. 31, 1153 (1973).

15. S. J. Brodsky, AIP Conf. Proc. No. 15, High Energy Collisions, 1973 (Stony Brook), American Institute of Physics, N.Y.

16. R. L. Anderson, B. Gottschalk, D. B. Gustavson, D. M. Ritson, G. A. Weitsch, H. J. Halpern, R. Prepost, and D. H. Tompkins. Phys. Rev. Lett. 30, 627 (1973).

17. G. Buschhorn, J. Carroll, R. D. Eandi, P. Heide, R. Hubner, W. Kern, U. Kotz, P. Schmüser, and H. J. Skronn, Phys. Rev. Lett. 18, 571 (1967).

18. R. P. Feynman, Photon-Hadron Interactions (W. A. Benjamin, New York, 1972).

19. M. Gronau, F. Ravndal and Y. Zarmi, Nucl. Phys. B51, 611 (1973).

20. J. T. Dakin and G. J. Feldman, Phys. Rev. D8, 2862 (1973).

21. C. J. Bebek, C. N. Brown, M. Herzlinger, S. D. Holmes, C. A. Lichtenstein, F. M. Pipkin, S. Raither and L. K. Sisterson, Phys. Rev. Lett. 34, 759 (1975). The π^+/π^- ratios presented in this paper cover smaller $p_\perp^2$ range than those given here.

22. C. J. Bebek, C. N. Brown, M. Herzlinger, S. Holmes, C. A. Lichtenstein, F. M. Pipkin, S. Raither and L. K. Sisterson, Phys. Rev. Lett. 34, 1115 (1975).

23. R. Blankenbecler, S. J. Brodsky and J. F. Gunion, Phys. Lett. 42B, 461 (1972) and Phys. Rev. D6, 2652 (1972).

24. We have divided $E\frac{d\sigma}{d^3p}$ by σ_{tot} principally to remove the rather large Q^2 dependence present in the electroproduction data. This is, perhaps, not a strictly correct interpretation of the parton interchange model prediction. However, σ_{tot} has only a slight W dependence in our range of

measurements. The effect on n in eq. 14 of dividing by σ_{tot} is to reduce n by about 0.6 in our low Q^2 region where most of the data lie.

25. J. W. Cronin, H. J. Frisch, M. J. Shocet, J. P. Boymond, P. A. Pirone and R. L. Sumner, Phys. Rev. Lett. 31, 1426 (1973) and F. W. Busser, L. Camilleri, L. DiLella, G. Gladding, A. Placci, B. G. Pope, A. M. Smith, J. K. Yoh, E. Zavattini, B. J. Blumenfeld, L. M. Lederman, R. L. Cool, L. Litt and S. L. Segler, Phys. Lett. 46B, 471 (1973).

26. K. C. Moffeit, J. Ballam, G. B. Chadwick, M. Della-Negra, R. Gearhart, J. J. Murray, P. Seyboth, C. K. Sinclair, I. O. Skillicorn, H. Spitzer, G. Wolf, H. H. Bingham, W. B. Fretter, W. J. Podolsky, M. S. Rabin, A. H. Rosenfeld, R. Windmolders, G. P. Yost, and R. H. Milburn, Phys. Rev. D5, 1603 (1972), SLAC-PUB-1004 (1971) and Phys. Rev. D5, 545 (1972).

27. L. W. Mo and Y. S. Tsai, Rev. Mod. Phys. 41, 205 (1969).

Figure Captions

1. Correspondence between Electroproduction and Virtual Photoproduction.
2. CM phase space regions covered by the Harvard-Cornell experiments.
3. Missing mass squared spectra obtained in forward pion production from H_2 and D_2.
4. Ratio of $\pi^- p$ yield to $\pi^+ n$ yield from deuterium versus momentum transfer.
5. The pion form factor dependence upon the minimum momentum transfer at fixed Q^2.
6. The pion form factor versus Q^2.
7. Center of mass angular distribution for single pion virtual photoproduction.
8. W dependence of $\gamma_v + p \to \pi^+ + n$ for fixed Q^2 at four CM angles.
9. Q^2 dependence of $\gamma_v + p \to \pi^+ + n$ for two W intervals. The data at $\theta^* = 0°$ are from Ref. 3 while the photoproduction measurements are from Ref. 16 and 17.
10. The invariant structure function for $\pi^\pm$ virtual photoproduction from protons for $P_\perp^2 < 0.02$ GeV^2.
11. The π^+ structure function from protons divided by the fit equation 12. Data are restricted to $p_\perp^2 < 0.02$ GeV^2. Radiative corrections have been applied to data.
12. The π^+ and π^- structure functions from neutrons for $p_\perp^2 < 0.02$ GeV^2 divided by the fit equation 11.
13. The ratio of the number of π^+ to π^- from protons versus x' for $p_\perp^2 < 0.02$ GeV^2.
14. π^+/π^- ratio from neutrons versus x' for $p_\perp^2 < 0.02$ GeV^2.
15. π^+/π^- ratio from protons versus $p_\perp^2$ for $0.5 < x' < 0.7$.
16. π^+/π^- ratio from protons and neutrons averaged over intervals $P_\perp^2 < 0.2$ GeV^2 and $0.3 < x' < 0.7$. Ratios are displayed as functions of $1/\omega$ and W.

17. The invariant structure function for proton virtual photoproduction from proton and neutron targets.

18. The invariant structure function for K^+ mesons for $p_\perp^2 < 0.05$ GeV^2. The solid curve is 0.20 times the fit to the invariant structure functions for π^+ with $p_\perp^2 < 0.02$.

19. The π^+ invariant structure function near $x = 0$ versus $x_\perp$. The solid curves represent a fit to the data which contains no Q^2 dependence.

20. The W dependence of the π^+ invariant structure function at $x = 0$ shown as a function of $x_\perp$.

21. $\frac{d\sigma}{d\Omega^* dM_x^2}$ versus M_x^2 at $Q^2 = 1.2$ GeV^2 for three W intervals. The curves represent a W^n dependence.

22. The π^+ invariant structure function near $x = 0$ versus $p_\perp^2$ at $Q^2 = 1.2$ GeV^2.

23. The π^- invariant structure function near $x = 0$ versus $p_\perp^2$ at W= 3.1 GeV for $Q^2 = 1.2$ GeV^2 compared with the photoproduction measurements of Ref. 26.

24. π^+/π^- ratio versus $x_\perp$ near $x = 0$ for several (Q^2, W) values. The dashed lines are the average ratio for each figure.

25. π^+/π^- ratio from protons near $x = 0$ averaged over all $x_\perp$ displayed as functions of $1/\omega$ and W.

26. The proton missing mass squared spectrum obtained for W= 2.15 GeV and $Q^2 = 1.2$ GeV^2. The curves represent a preliminary fit to the data.

27. The proton invariant structure function at $x = 0.4$ versus $x_\perp$ for various (Q^2, W) points. The curves are independent of Q^2.

28. The W dependence of the proton invariant structure function at $x = 0.4$ plotted as a function of $x_\perp$.

29. The proton invariant structure function versus $p_\perp^2$.

30. The radiative correction to the invariant structure functions for pions produced along the virtual photon direction.

31. The radiative correction to the structure functions for pions produced at $x = 0$.

Electroproduction $\longleftrightarrow$ Virtual Photoproduction

$e+p \rightarrow e+h+x$ $\qquad$ $\gamma_v + p \rightarrow h+x$

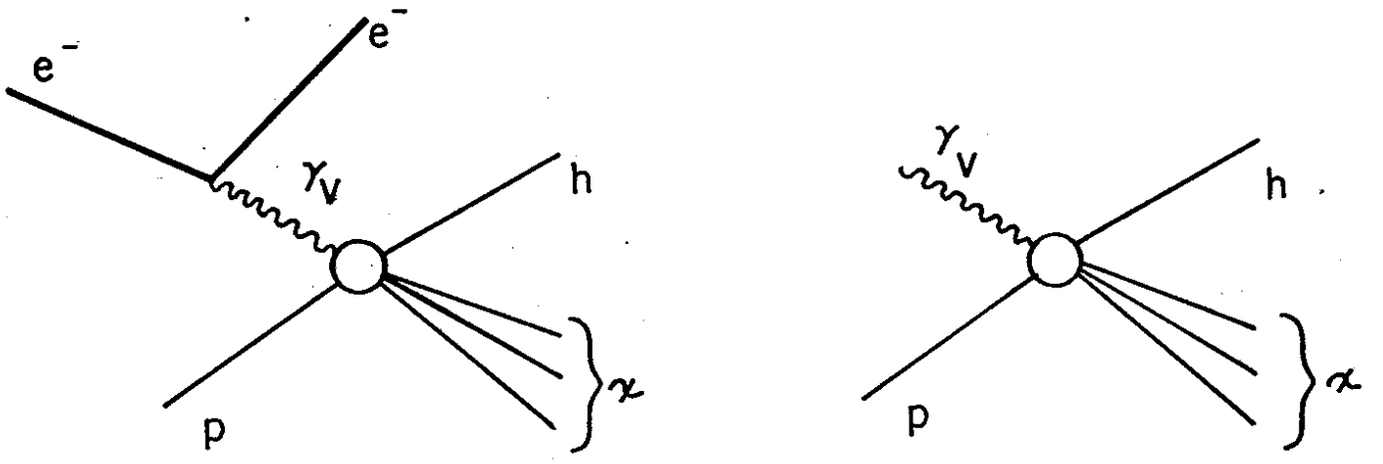

$$\frac{d\sigma}{d\Omega_e\, dE'_e\, d^3p_h} \qquad \Gamma \frac{d\sigma}{d^3p_h}$$

$$\Gamma = \frac{\alpha}{4\pi^2 Q^2} \frac{E'}{E} \frac{(W^2 - M^2)}{M(1-\epsilon)}$$

$$\epsilon = \left[1 + 2\left[\frac{\nu^2 + Q^2}{Q^2}\right] \tan^2 \frac{\theta_e}{2}\right]^{-1}$$

Figure 1

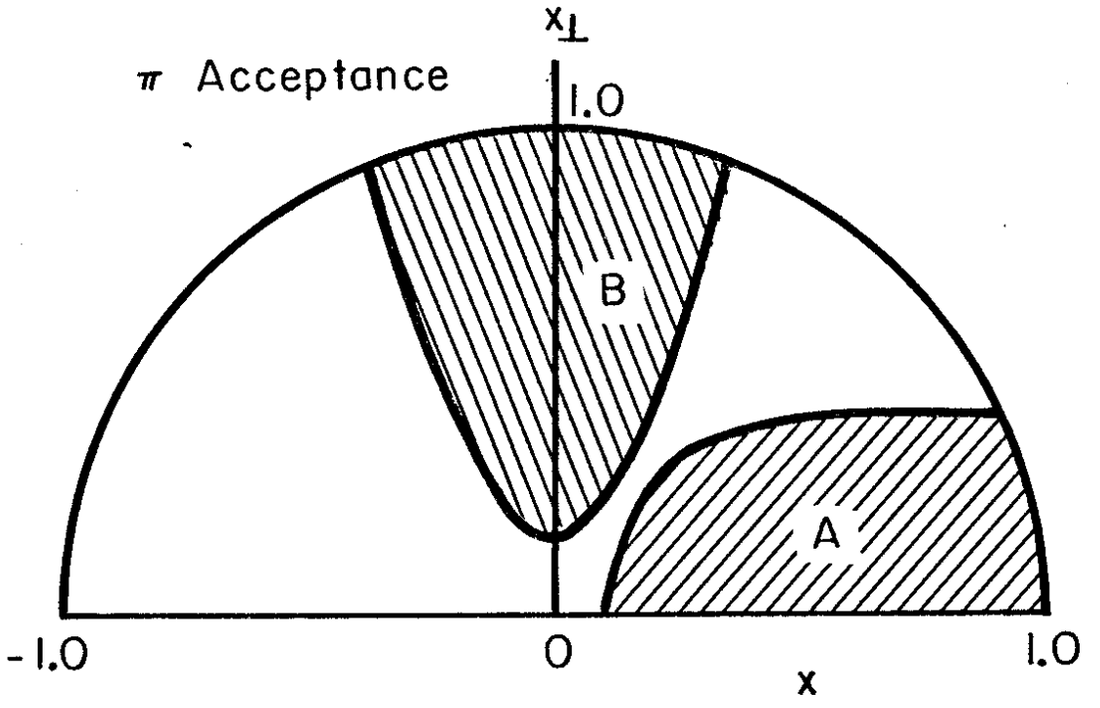

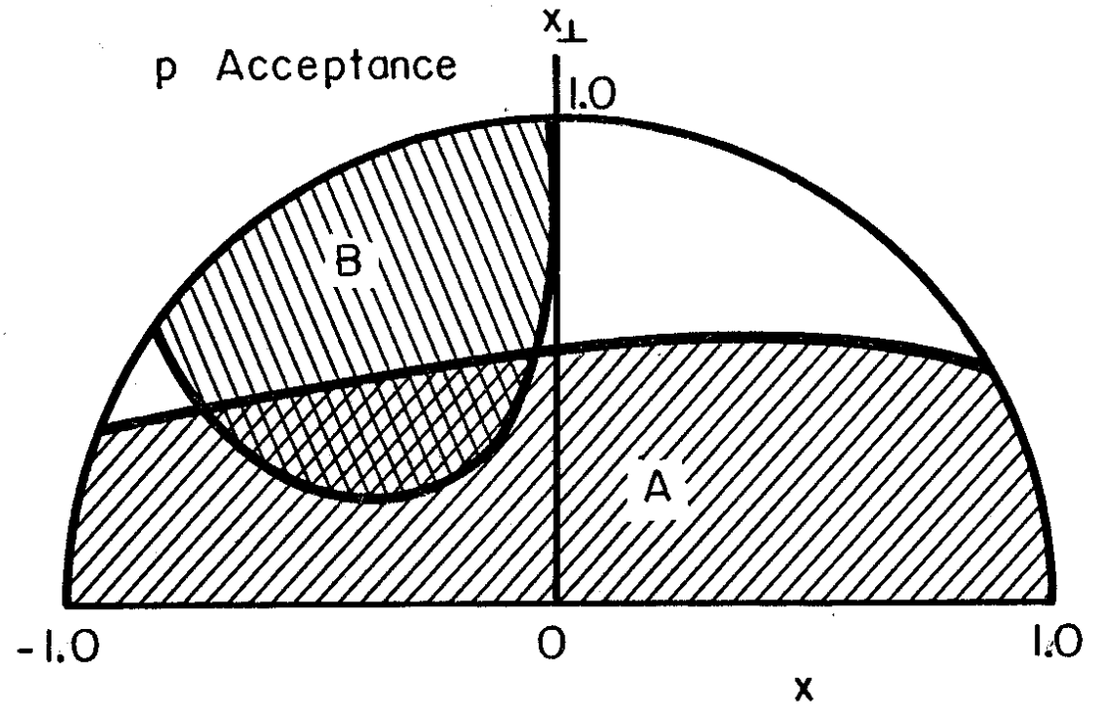

Figure 2

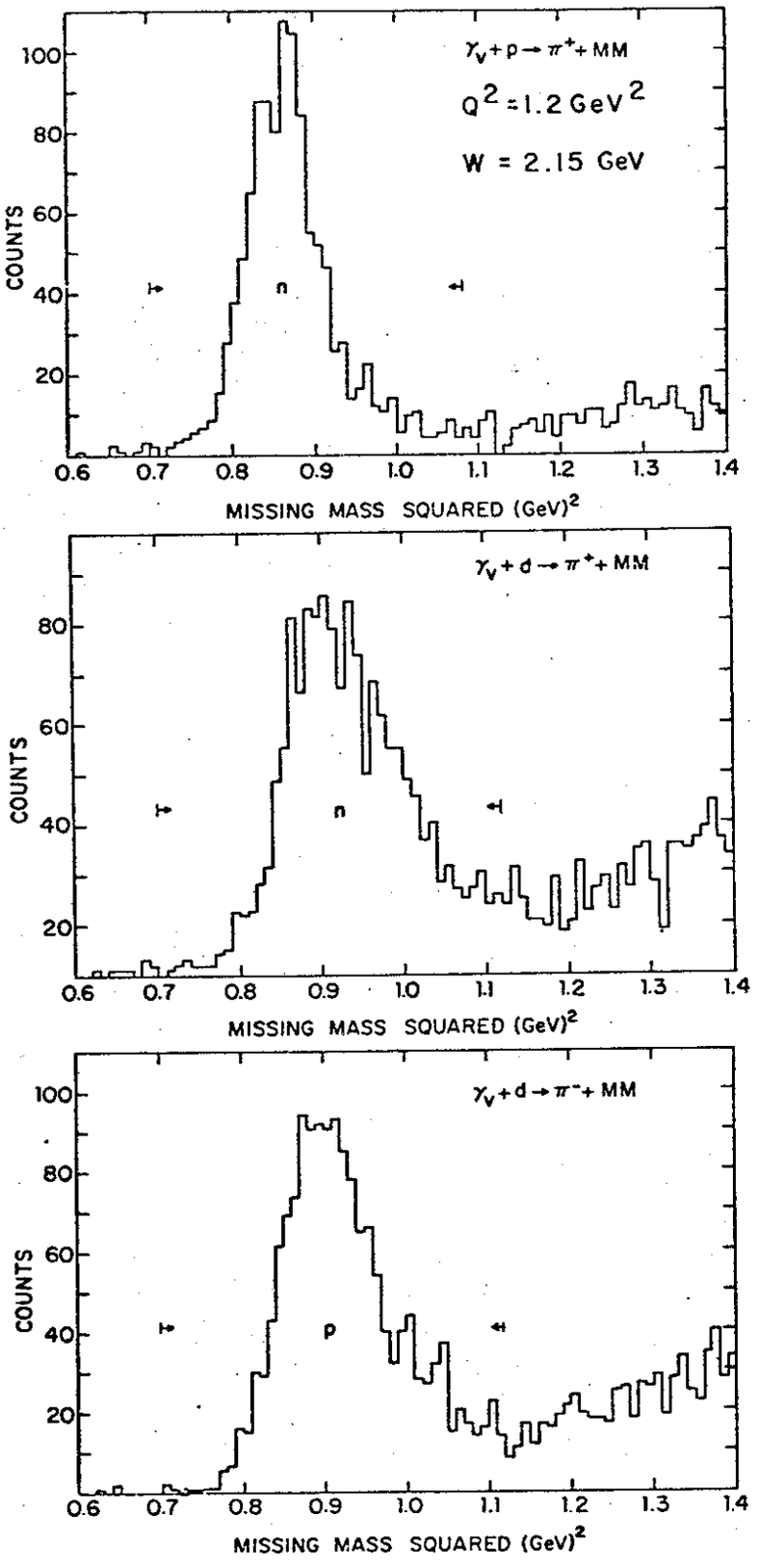
$\gamma_v + p \rightarrow \pi^+ + MM$
$Q^2 = 1.2\ GeV^2$
W = 2.15 GeV
COUNTS
n
MISSING MASS SQUARED (GeV)^2
$\gamma_v + d \rightarrow \pi^+ + MM$
COUNTS
n
MISSING MASS SQUARED (GeV)^2
$\gamma_v + d \rightarrow \pi^- + MM$
COUNTS
p
MISSING MASS SQUARED (GeV)^2

Figure 3

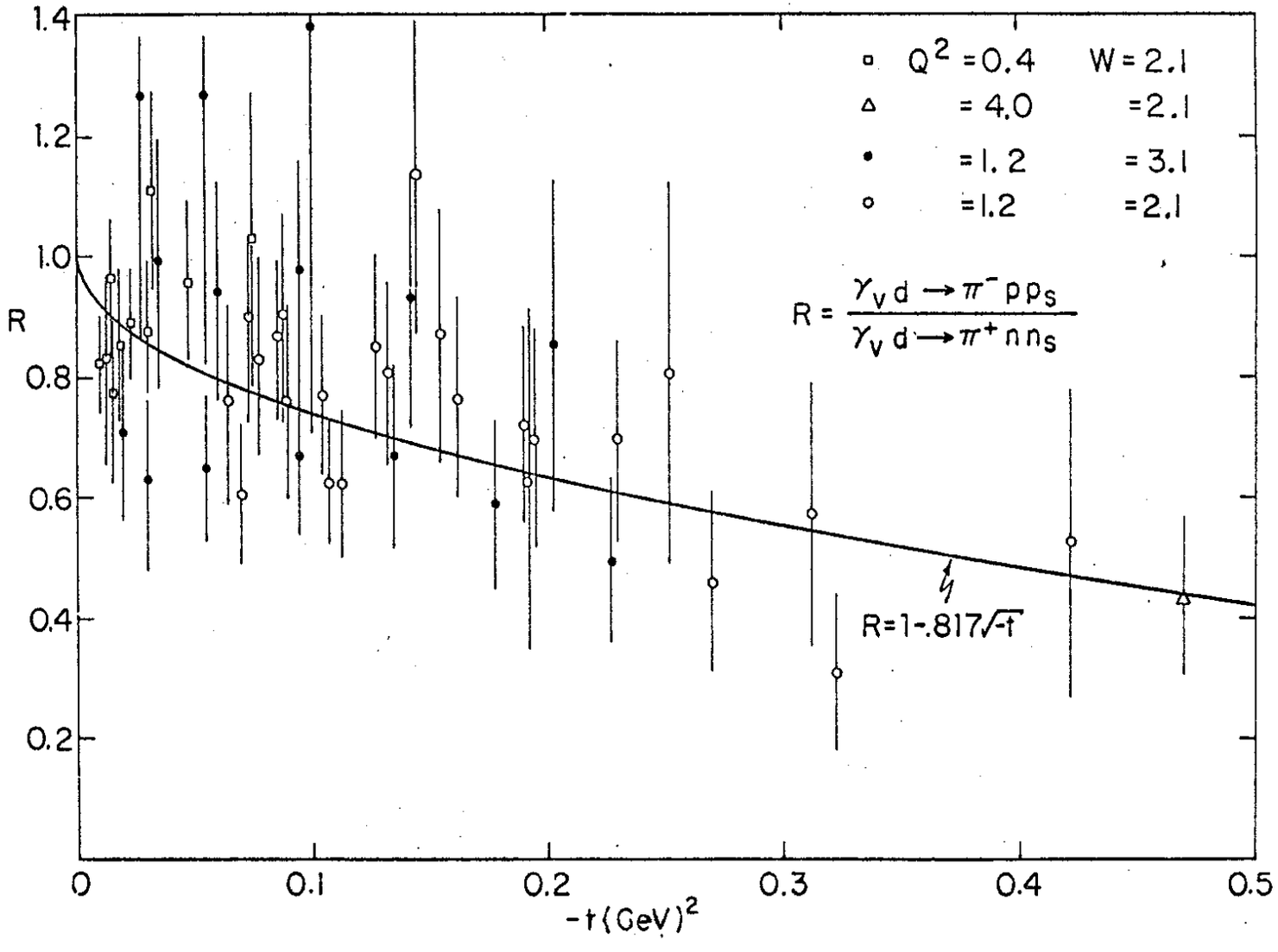
1.4
1.2
1.0
0.8
0.6
0.4
0.2
R
0
0.1
0.2
0.3
0.4
0.5
-t(GeV)²
□ Q² = 0.4 W = 2.1
△ = 4.0 = 2.1
• = 1.2 = 3.1
○ = 1.2 = 2.1
R = γv d → π⁻ pps / γv d → π⁺ nns
R=1-.817√-t

Figure 4

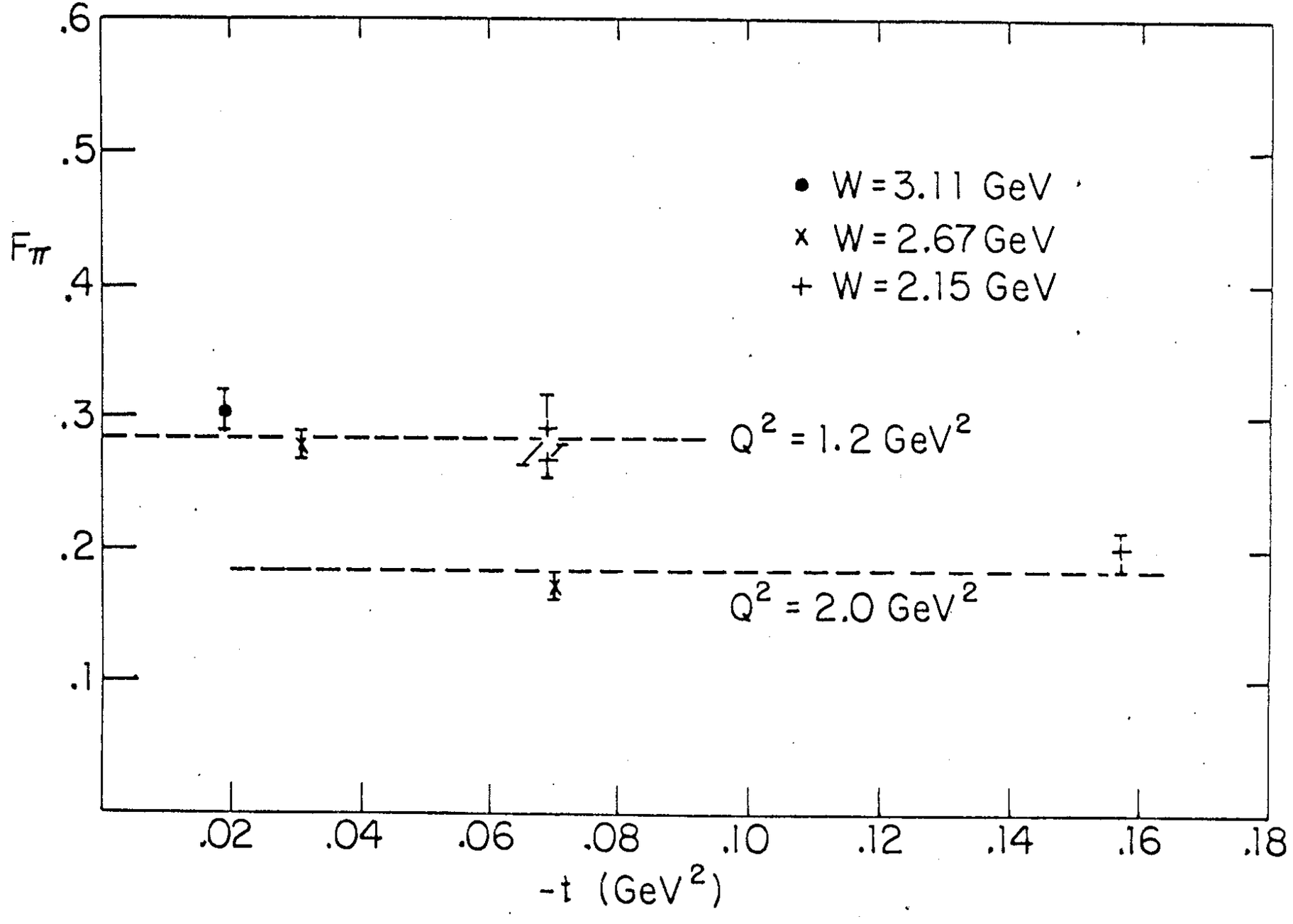
.6
.5
.4
.3
.2
.1
F_π
• W = 3.11 GeV
x W = 2.67 GeV
+ W = 2.15 GeV
Q^2 = 1.2 GeV^2
Q^2 = 2.0 GeV^2
.02
.04
.06
.08
.10
.12
.14
.16
.18
-t (GeV^2)

Figure 5

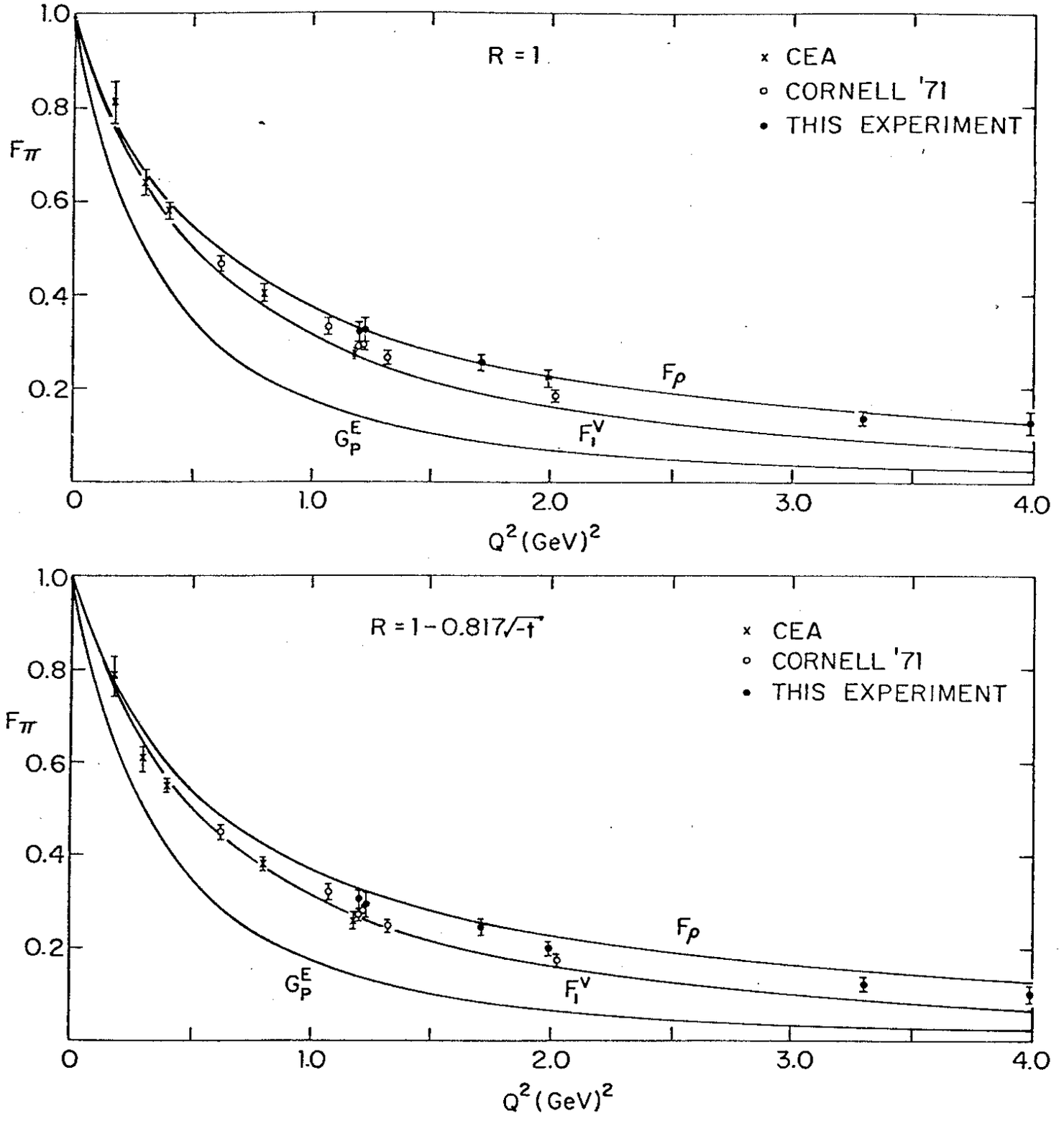
R = 1
× CEA
○ CORNELL '71
• THIS EXPERIMENT
F_π
F_ρ
G_P^E
F_1^V
1.0
0.8
0.6
0.4
0.2
0
1.0
2.0
3.0
4.0
Q^2 (GeV)^2

R = 1 − 0.817$\sqrt{-t}$
× CEA
○ CORNELL '71
• THIS EXPERIMENT
F_π
F_ρ
G_P^E
F_1^V
1.0
0.8
0.6
0.4
0.2
0
1.0
2.0
3.0
4.0
Q^2 (GeV)^2

Figure 6

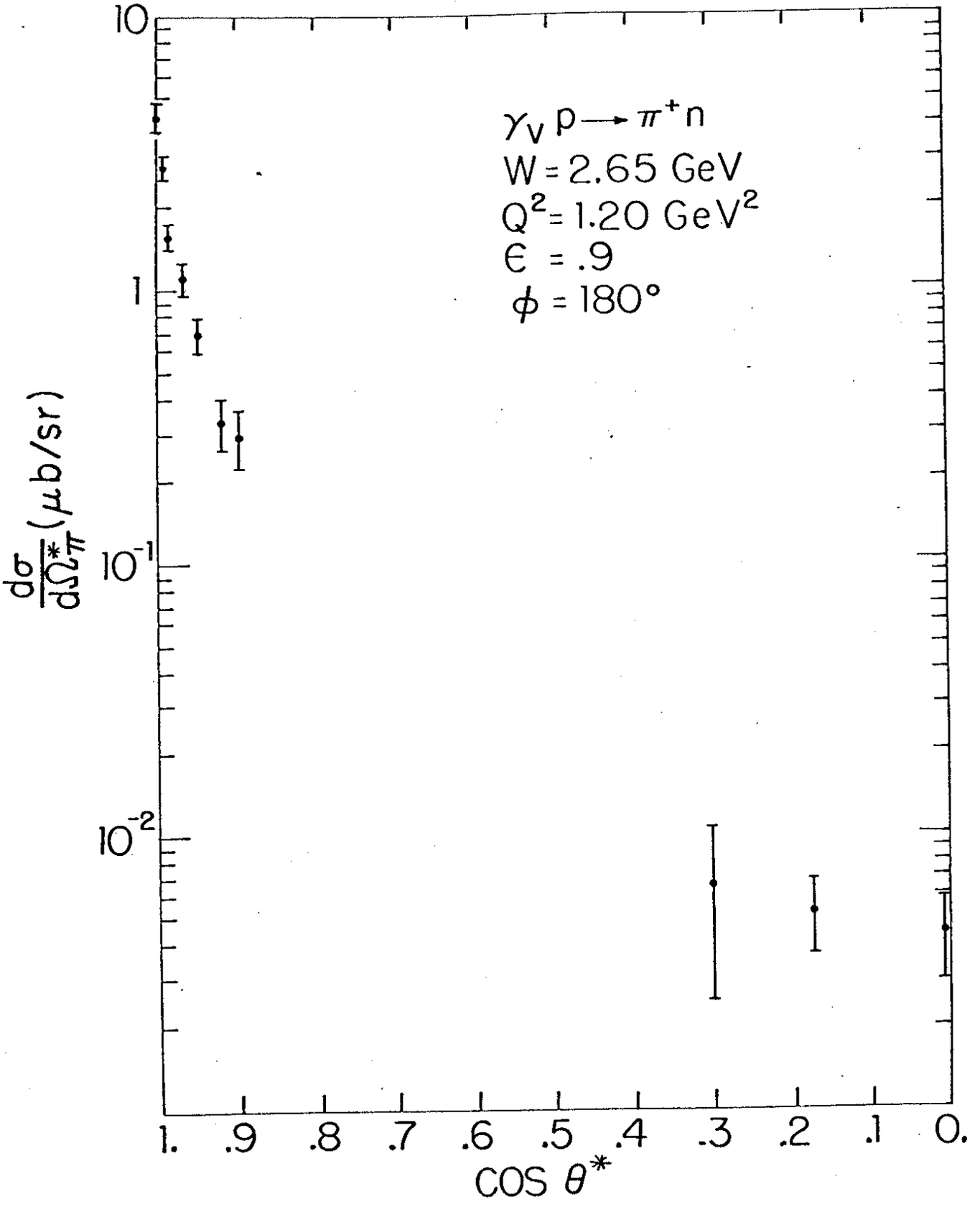
$\gamma_V p \rightarrow \pi^+ n$
W = 2.65 GeV
Q^2 = 1.20 GeV^2
ϵ = .9
ϕ = 180°
$\frac{d\sigma}{d\Omega^*_\pi}$ (μb/sr)
10
1
10^{-1}
10^{-2}
1.
.9
.8
.7
.6
.5
.4
.3
.2
.1
0.
COS θ^*

Figure 7

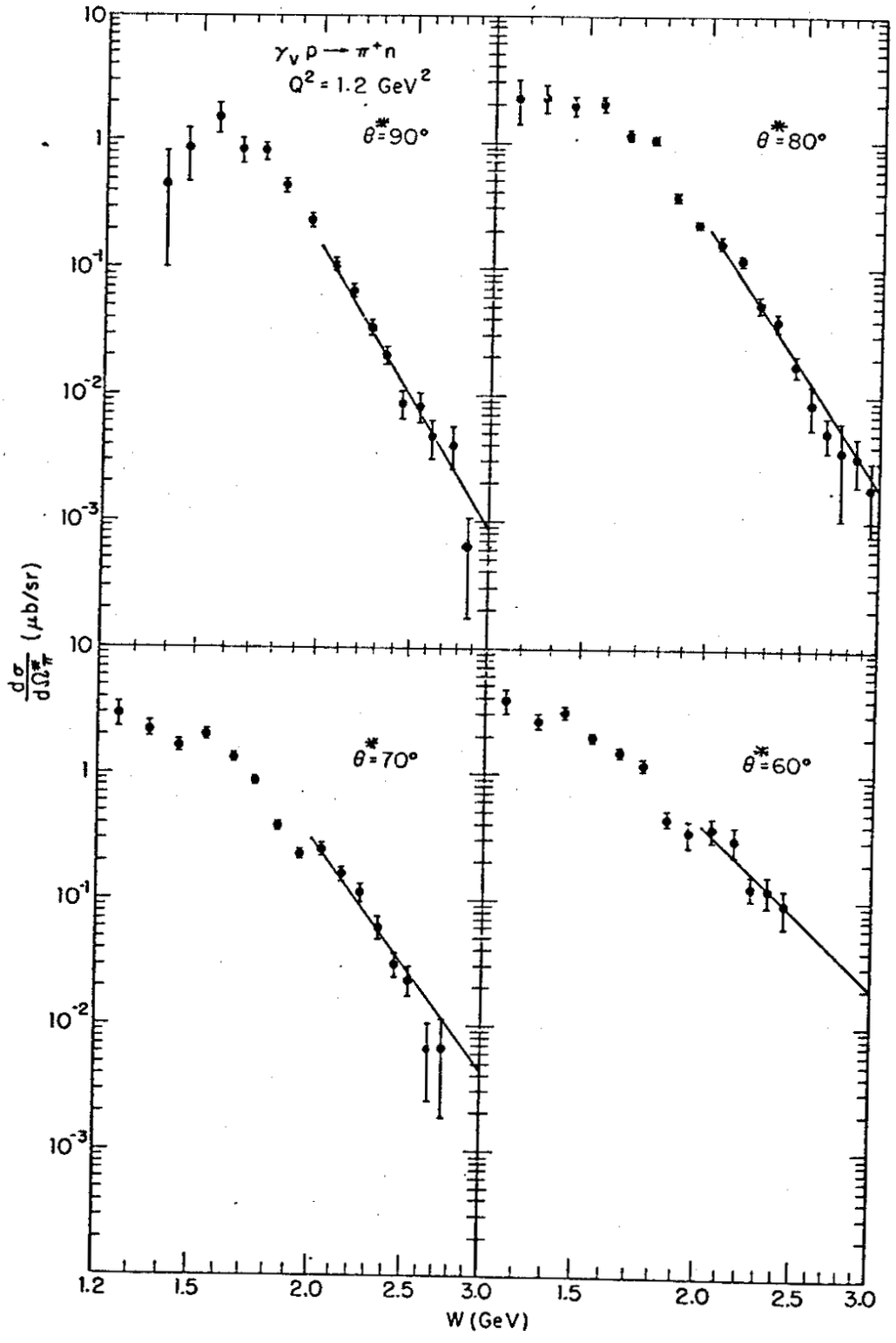
$\gamma_v p \rightarrow \pi^+ n$
$Q^2 = 1.2$ GeV^2
$\theta^*_\pi = 90°$
$\theta^*_\pi = 80°$
$\theta^*_\pi = 70°$
$\theta^*_\pi = 60°$
$\frac{d\sigma}{d\Omega^*_\pi}$ (μb/sr)
W (GeV)
10
1
10^{-1}
10^{-2}
10^{-3}
1.2
1.5
2.0
2.5
3.0

Figure 8

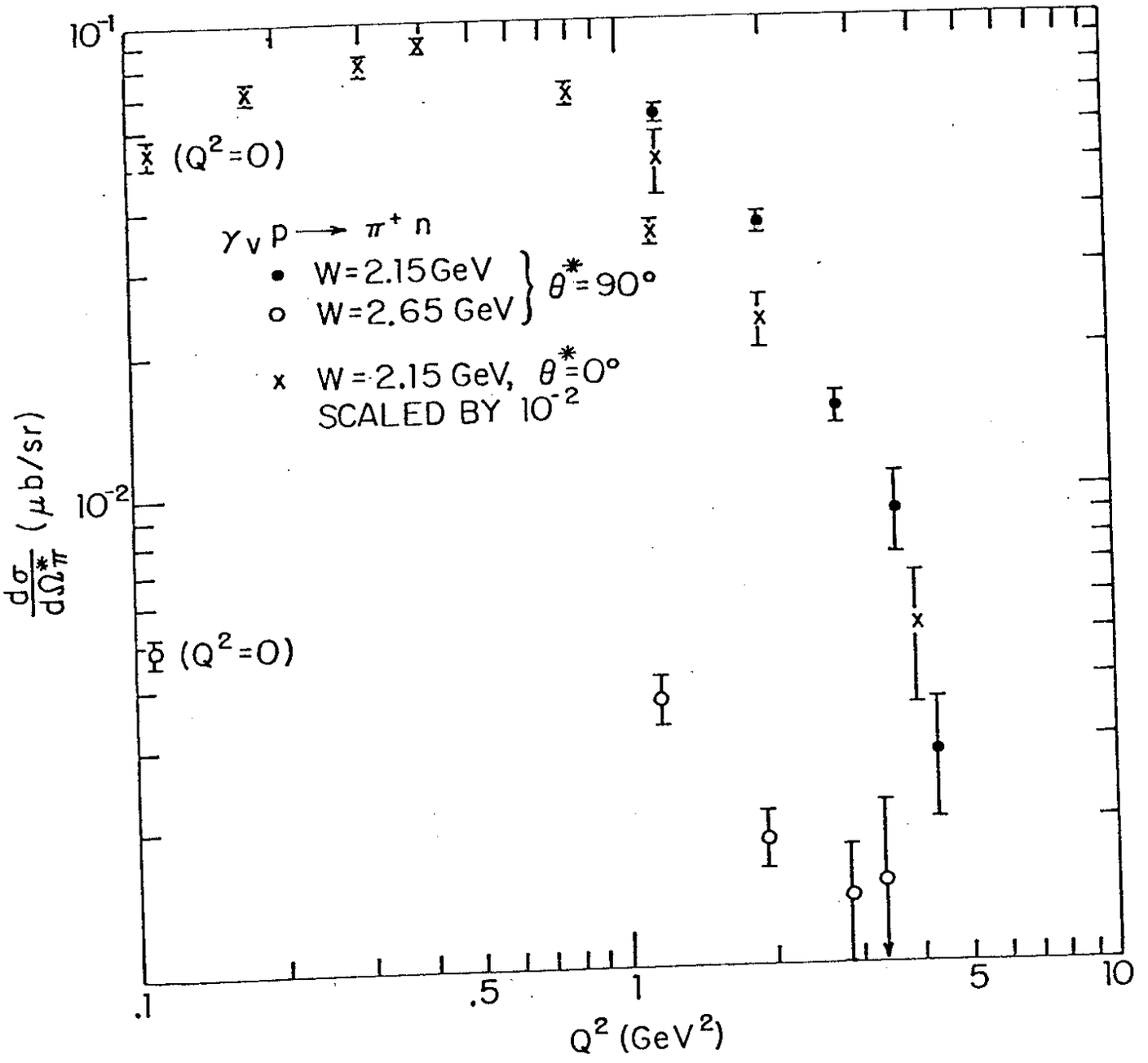
10^{-1}
10^{-2}
$(Q^2=0)$
$\gamma_V p \rightarrow \pi^+ n$
W=2.15GeV
W=2.65 GeV
$\theta^*=90°$
x W=2.15 GeV, $\theta^*=0°$
SCALED BY 10^{-2}
$(Q^2=0)$
$\frac{d\sigma}{d\Omega^*_\pi}$ (μb/sr)
.1
.5
1
5
10
Q^2 (GeV^2)

Figure 9

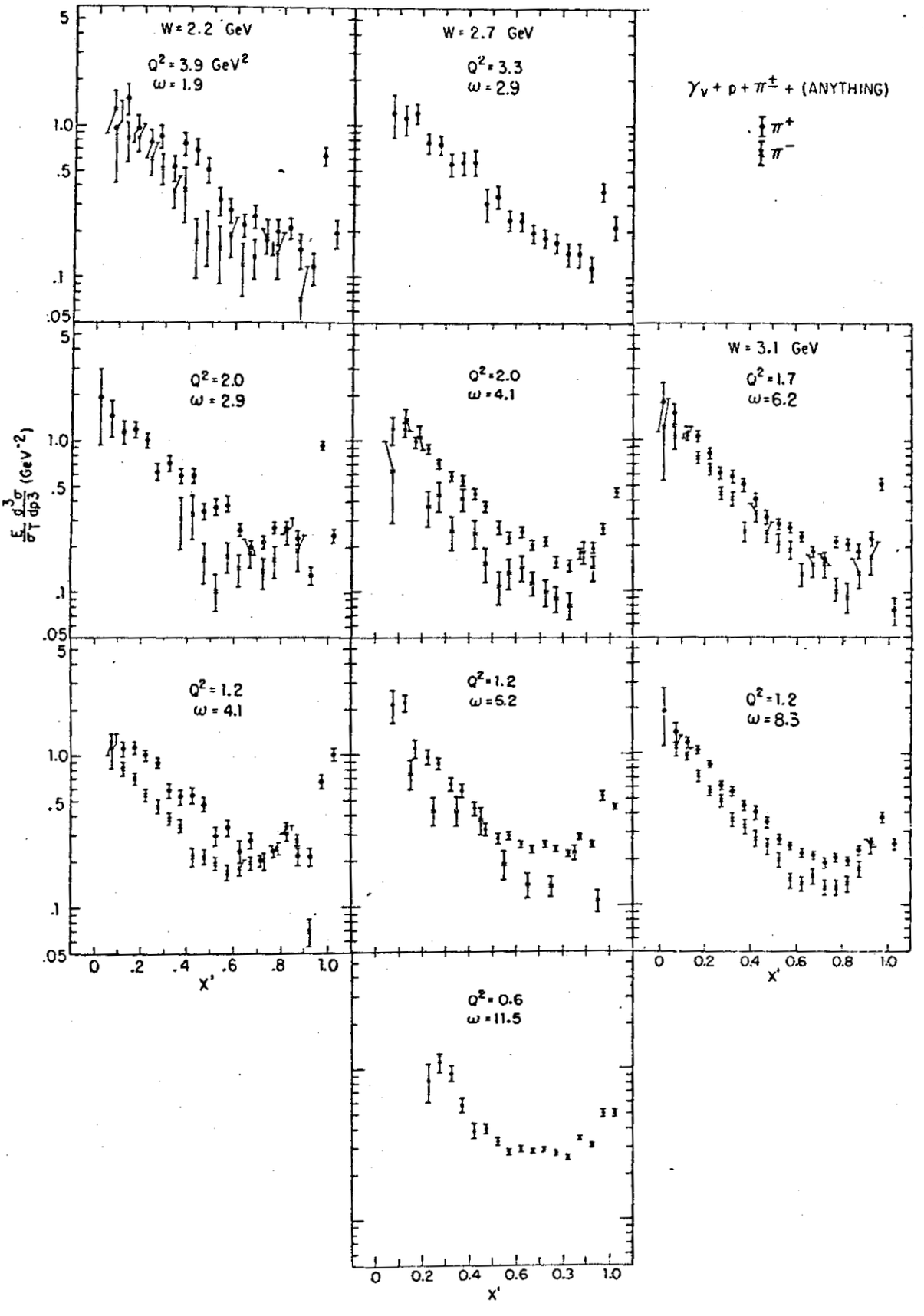
W = 2.2 GeV
Q² = 3.9 GeV²
ω = 1.9
W = 2.7 GeV
Q² = 3.3
ω = 2.9
γV + p + π± + (ANYTHING)
π+
π−
Q² = 2.0
ω = 2.9
Q² = 2.0
ω = 4.1
W = 3.1 GeV
Q² = 1.7
ω = 6.2
Q² = 1.2
ω = 4.1
Q² = 1.2
ω = 5.2
Q² = 1.2
ω = 8.3
Q² = 0.6
ω = 11.5
E/σT d³σ/dp³ (GeV⁻²)
x'

Figure 10

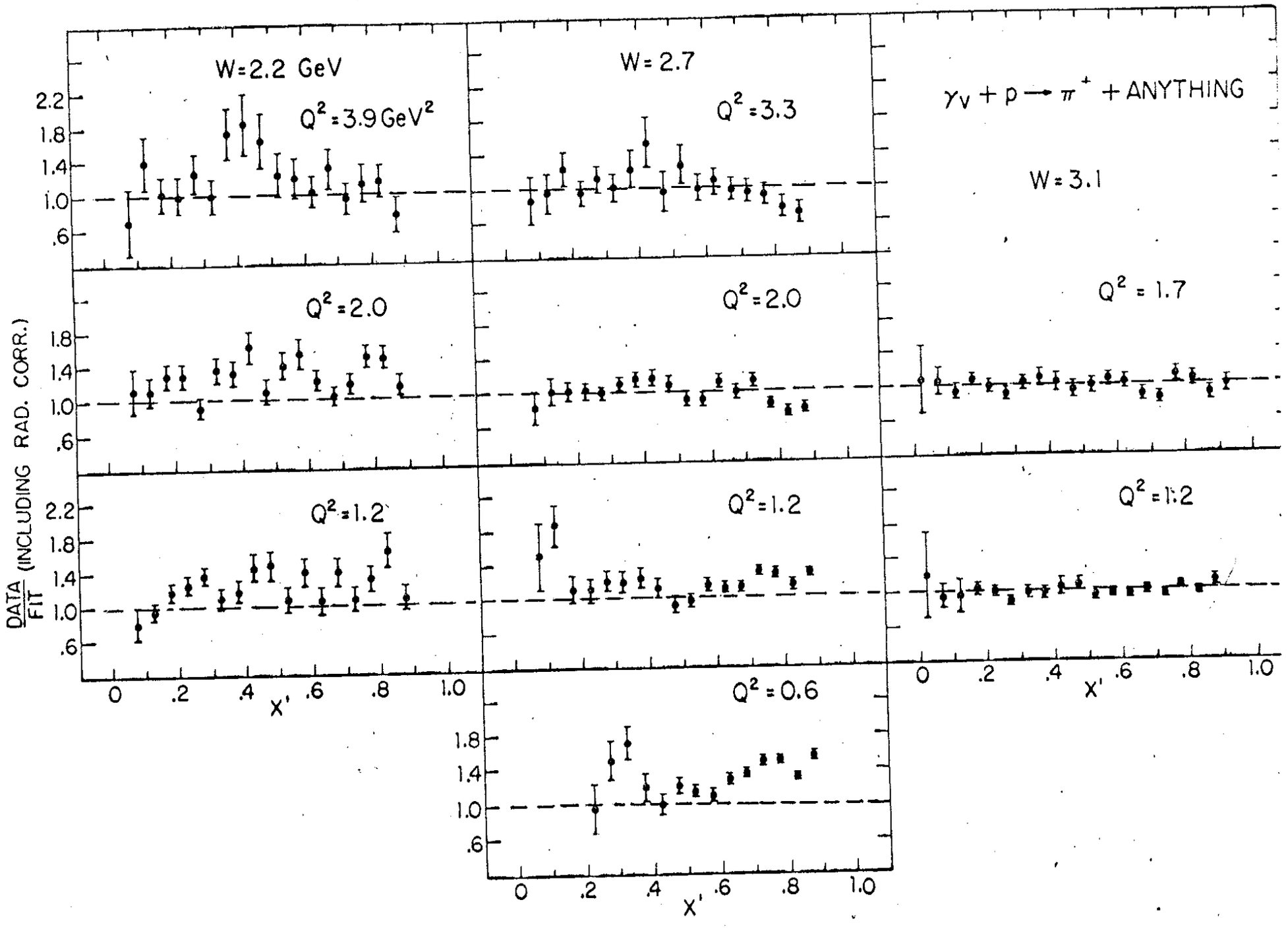
W=2.2 GeV
Q^2=3.9 GeV^2
W= 2.7
Q^2=3.3
$\gamma_V + p \rightarrow \pi^+ +$ ANYTHING
W= 3.1
Q^2=2.0
Q^2=2.0
Q^2 = 1.7
Q^2=1.2
Q^2=1.2
Q^2=1.2
Q^2 = 0.6
DATA/FIT (INCLUDING RAD. CORR.)
X'

Figure 11

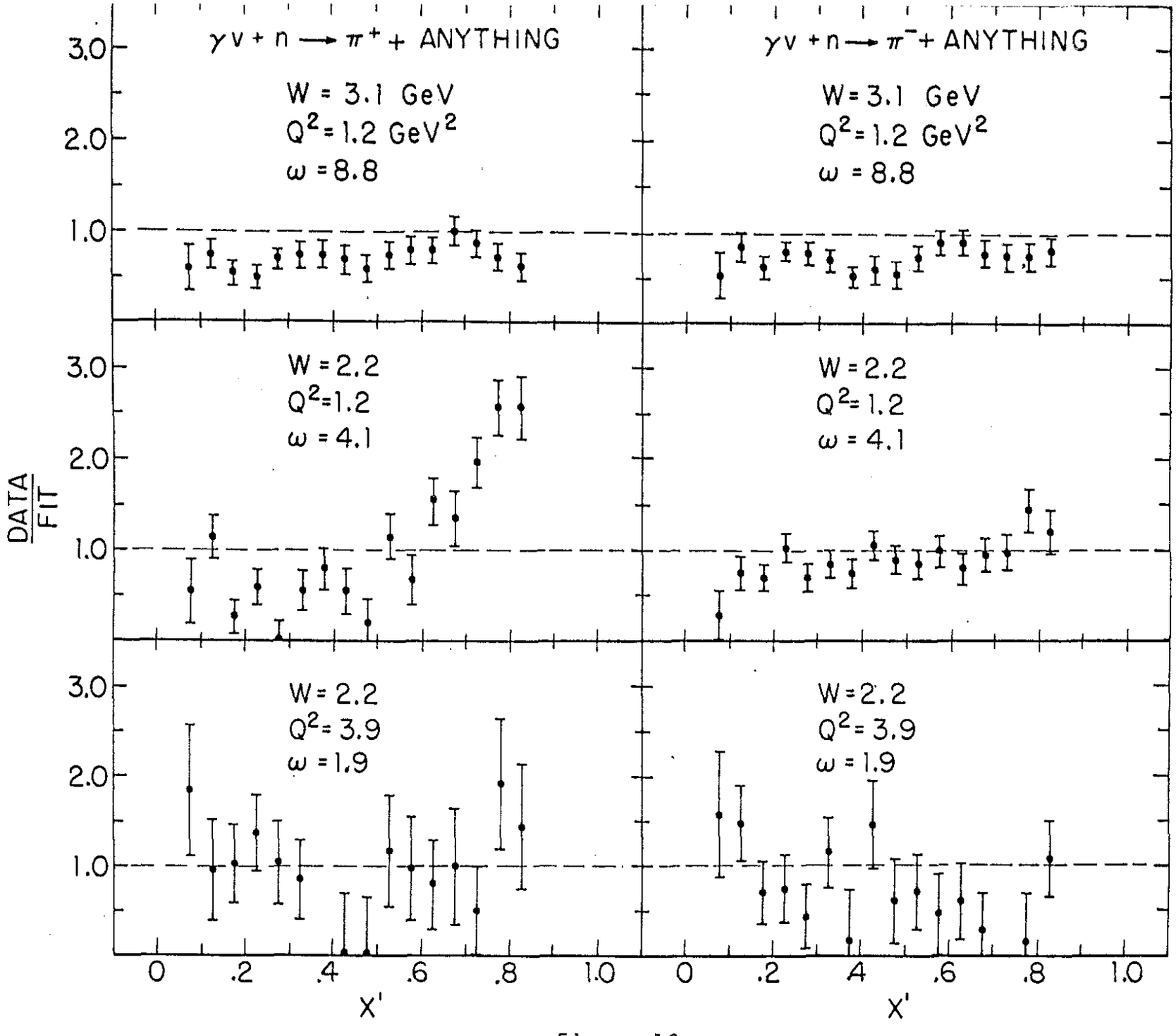
γν + n → π⁺ + ANYTHING
W = 3.1 GeV
Q² = 1.2 GeV²
ω = 8.8
γν + n → π⁻ + ANYTHING
W = 3.1 GeV
Q² = 1.2 GeV²
ω = 8.8
W = 2.2
Q² = 1.2
ω = 4.1
W = 2.2
Q² = 1.2
ω = 4.1
W = 2.2
Q² = 3.9
ω = 1.9
W = 2.2
Q² = 3.9
ω = 1.9
DATA/FIT
X'
X'

Figure 12

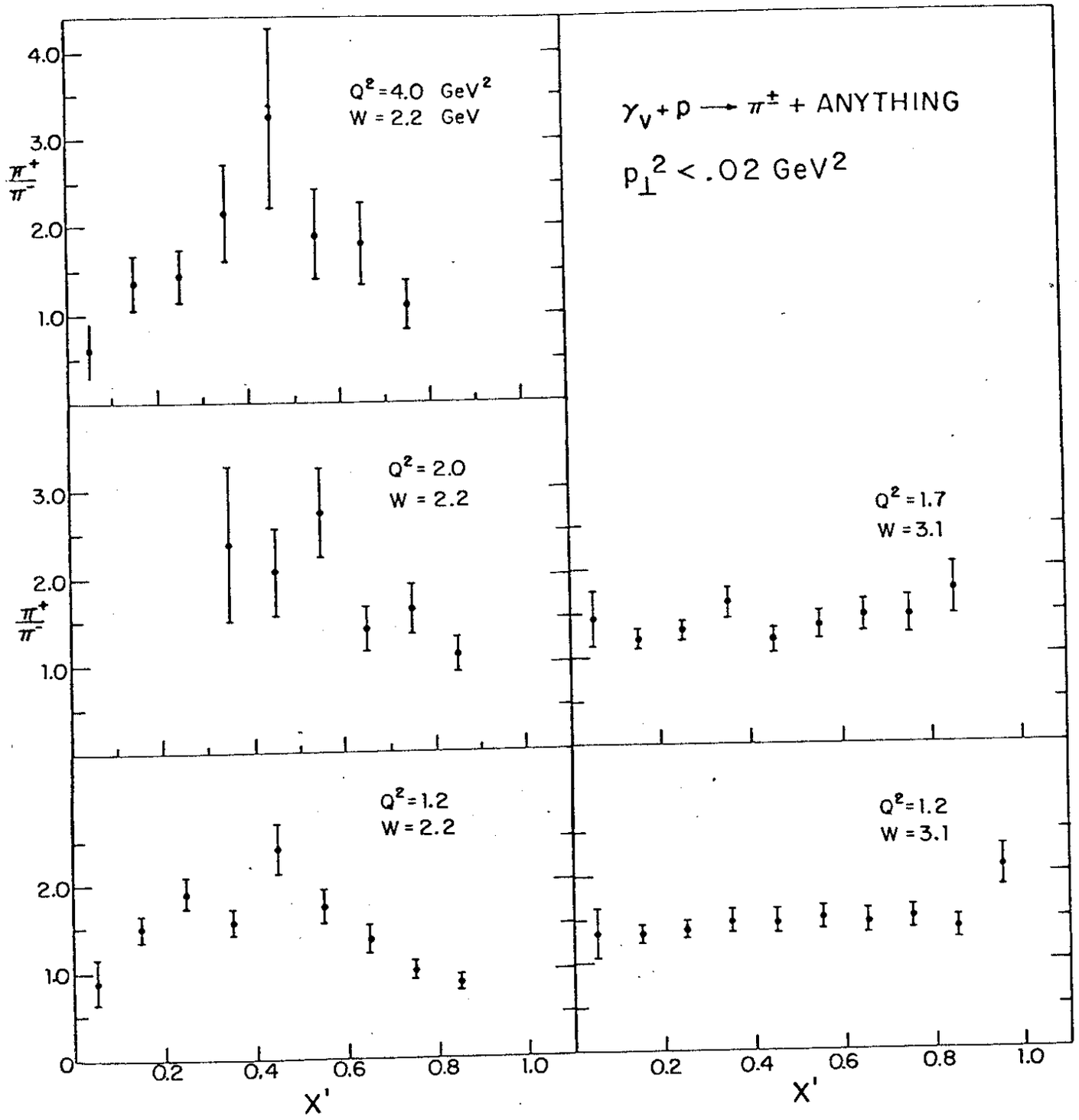
$\gamma_V + p \rightarrow \pi^{\pm}$ + ANYTHING
$p_\perp^2 < .02$ GeV^2
Q^2=4.0 GeV^2
W = 2.2 GeV
Q^2= 2.0
W = 2.2
Q^2= 1.7
W = 3.1
Q^2= 1.2
W = 2.2
Q^2= 1.2
W = 3.1
$\frac{\pi^+}{\pi^-}$
X'
0
1.0
2.0
3.0
4.0
0.2
0.4
0.6
0.8
1.0

Figure 13

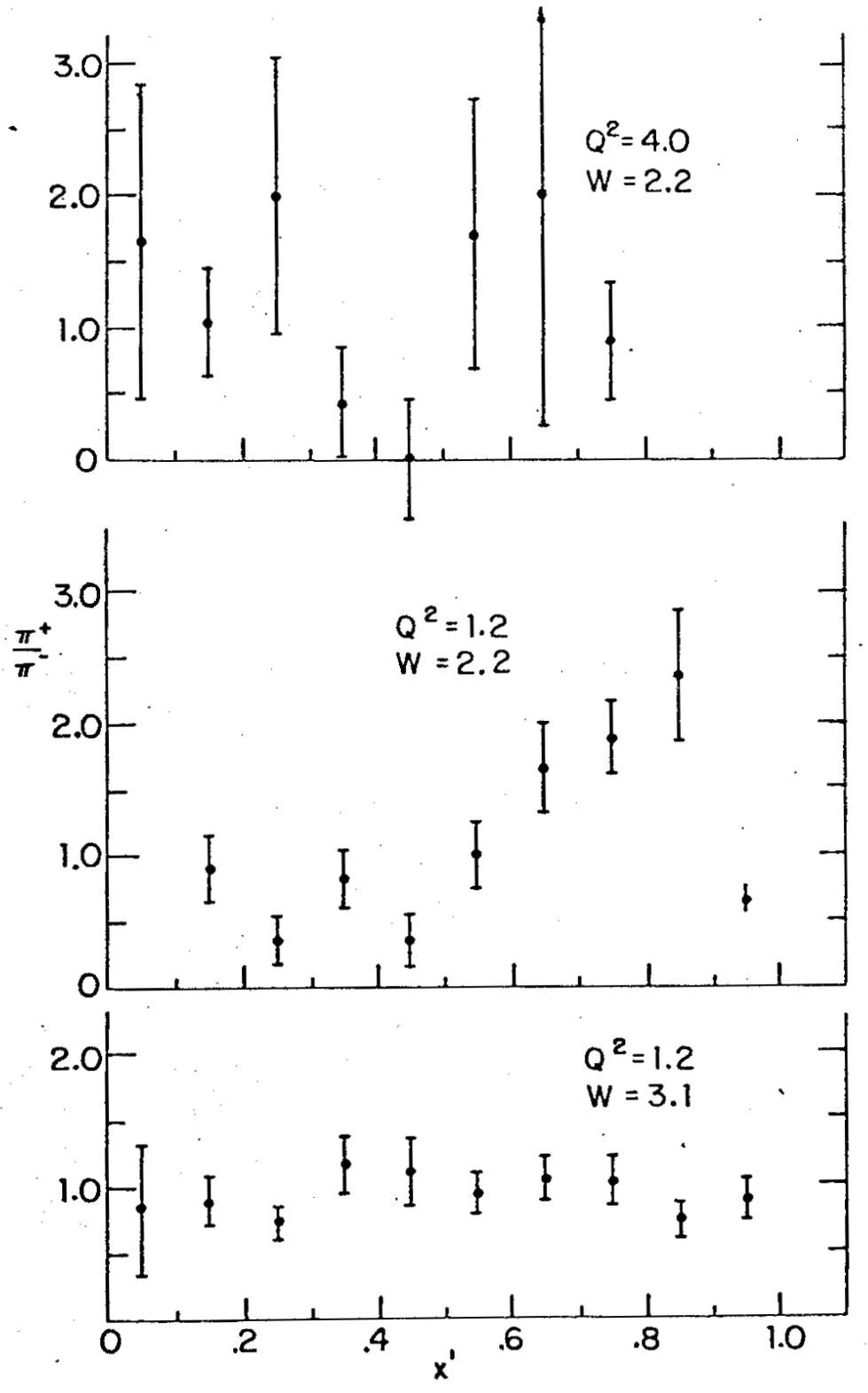
$\gamma_V + n \rightarrow \pi^{\pm}$ + anything
$p_\perp^2 < .02$ GeV^2
$Q^2 = 4.0$
$W = 2.2$
$Q^2 = 1.2$
$W = 2.2$
$Q^2 = 1.2$
$W = 3.1$
$\frac{\pi^+}{\pi^-}$
x'
0
.2
.4
.6
.8
1.0
1.0
2.0
3.0

Figure 14

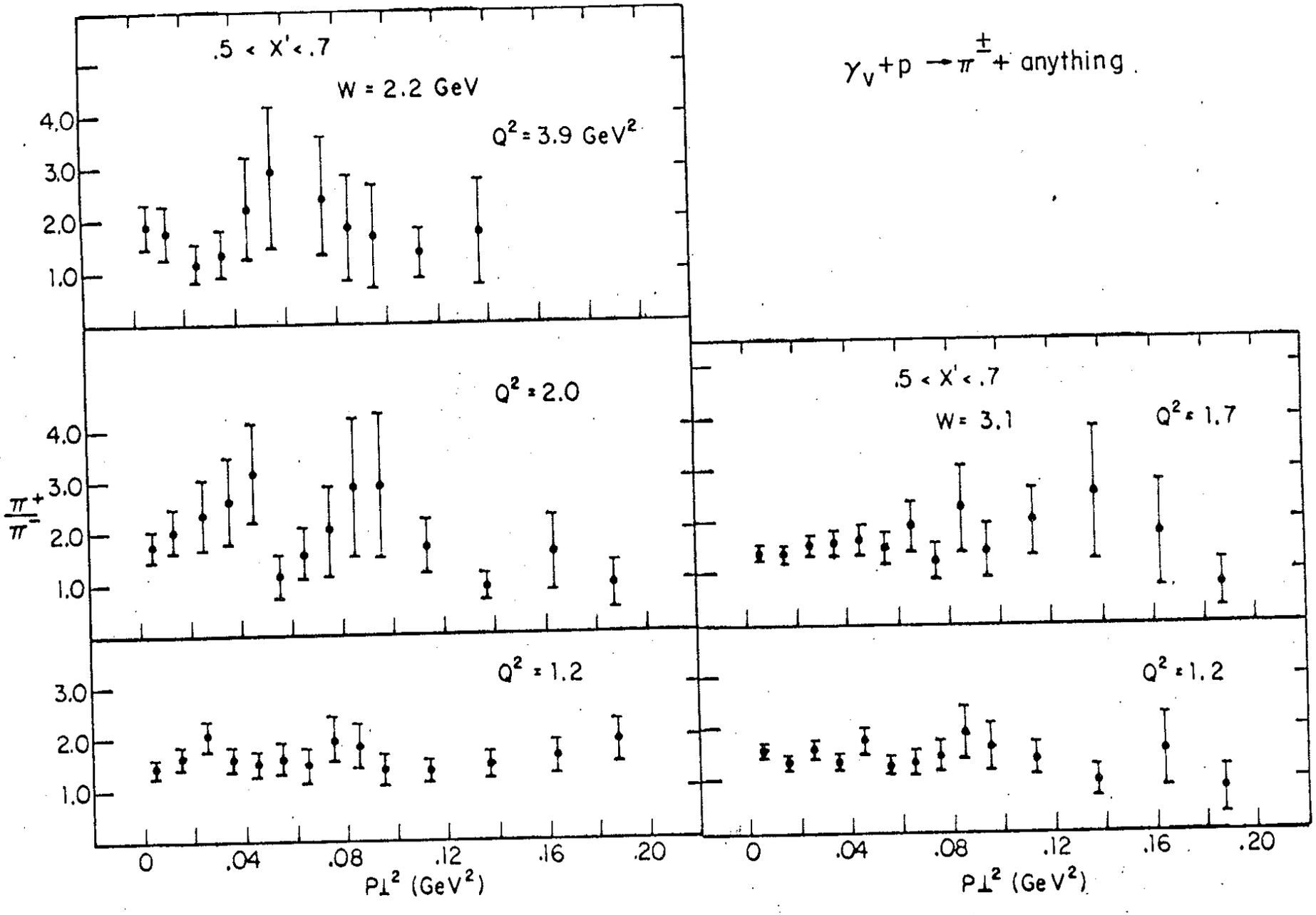
$\gamma_V + p \rightarrow \pi^{\pm}$ + anything
.5 < X' < .7
W = 2.2 GeV
Q^2 = 3.9 GeV^2
Q^2 = 2.0
Q^2 = 1.2
.5 < X' < .7
W = 3.1
Q^2 = 1.7
Q^2 = 1.2
$\frac{\pi^+}{\pi^-}$
1.0
2.0
3.0
4.0
0
.04
.08
.12
.16
.20
$P_\perp^2$ (GeV^2)

Figure 15

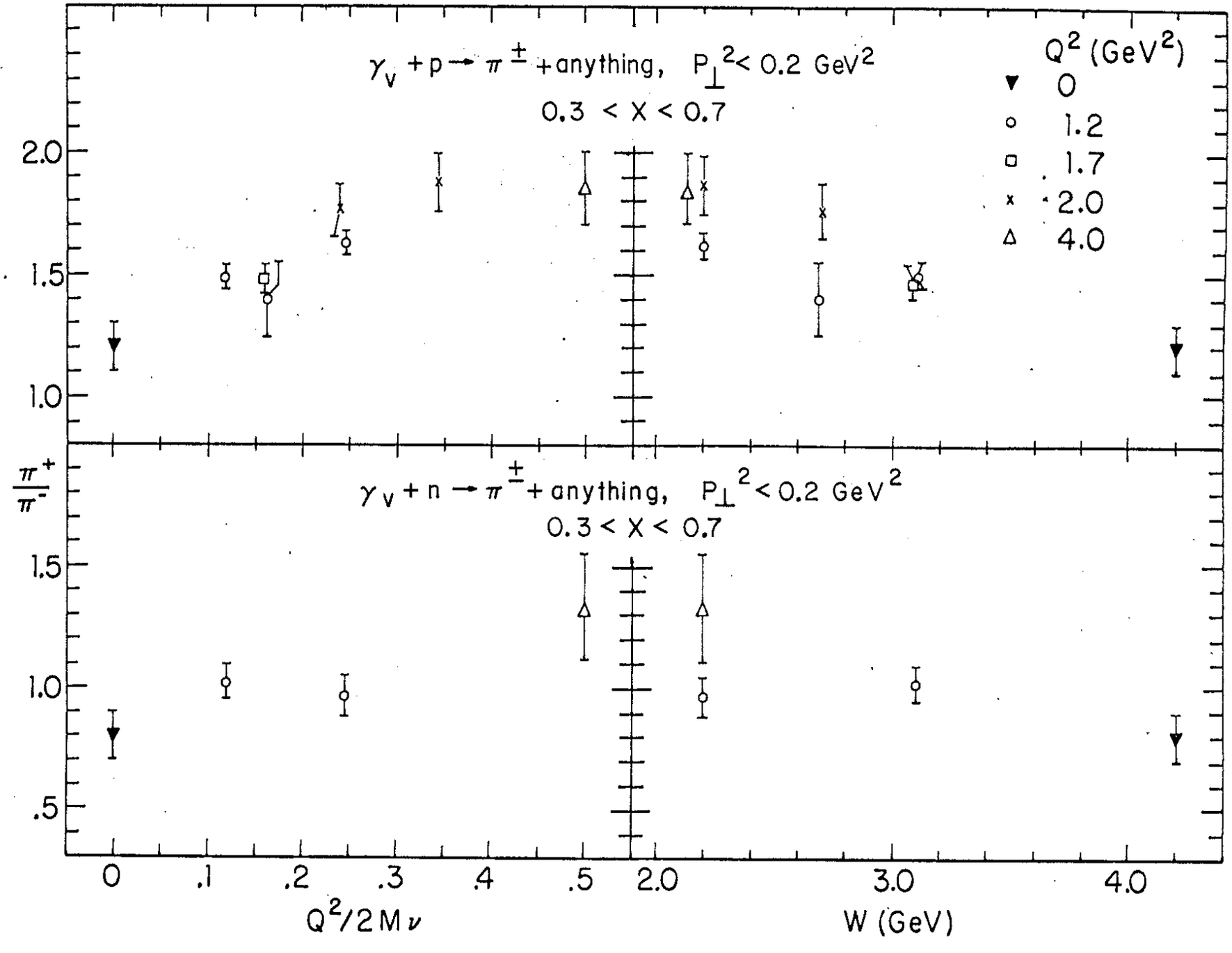

Figure 16

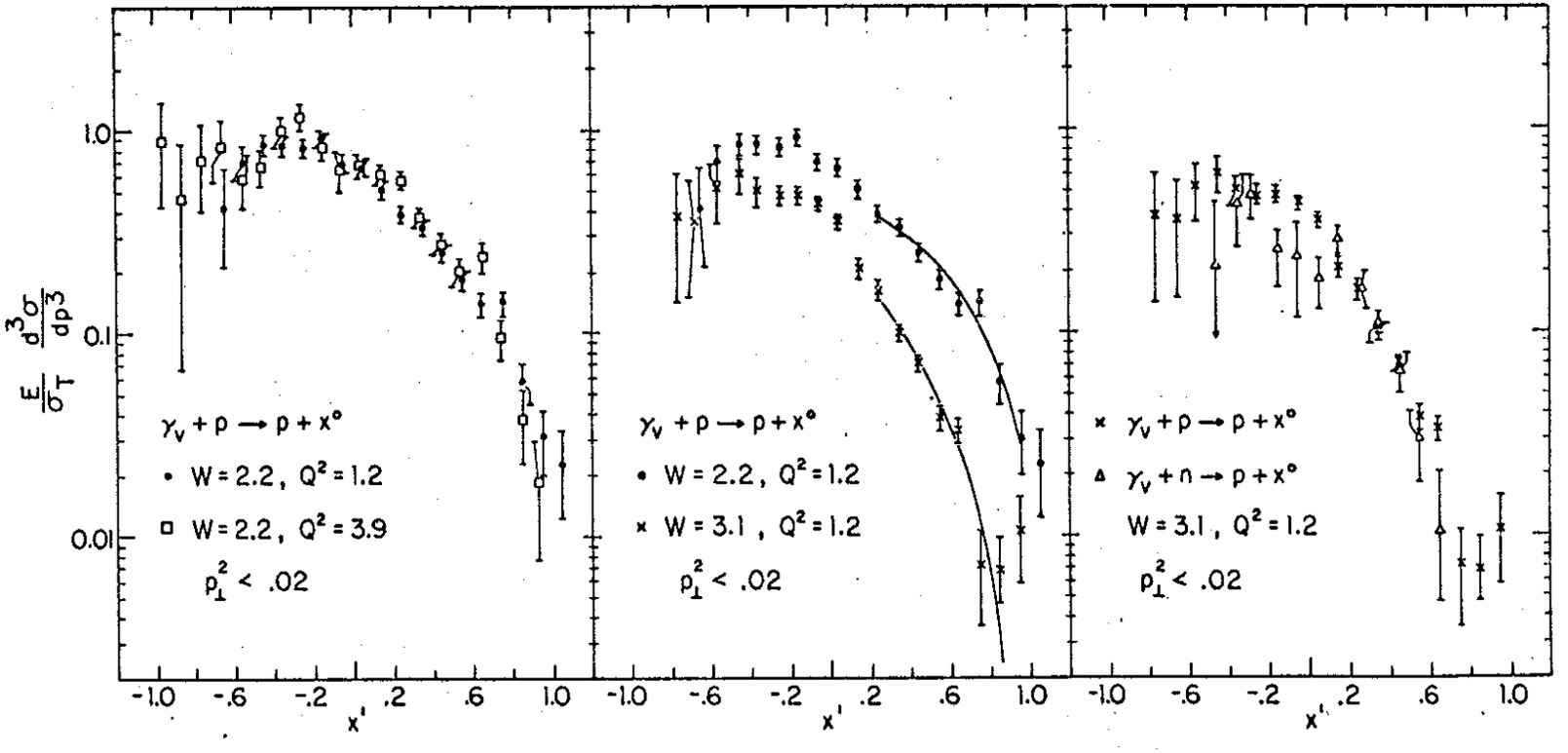
$\frac{E}{\sigma_T}\frac{d^3\sigma}{dp^3}$
1.0
0.1
0.01
$\gamma_V + p \rightarrow p + x^\circ$
• W = 2.2, Q^2 = 1.2
□ W = 2.2, Q^2 = 3.9
$p_\perp^2 < .02$
$\gamma_V + p \rightarrow p + x^\circ$
• W = 2.2, Q^2 = 1.2
× W = 3.1, Q^2 = 1.2
$p_\perp^2 < .02$
× $\gamma_V + p \rightarrow p + x^\circ$
△ $\gamma_V + n \rightarrow p + x^\circ$
W = 3.1, Q^2 = 1.2
$p_\perp^2 < .02$
-1.0 -.6 -.2 .2 .6 1.0
x'

Figure 17

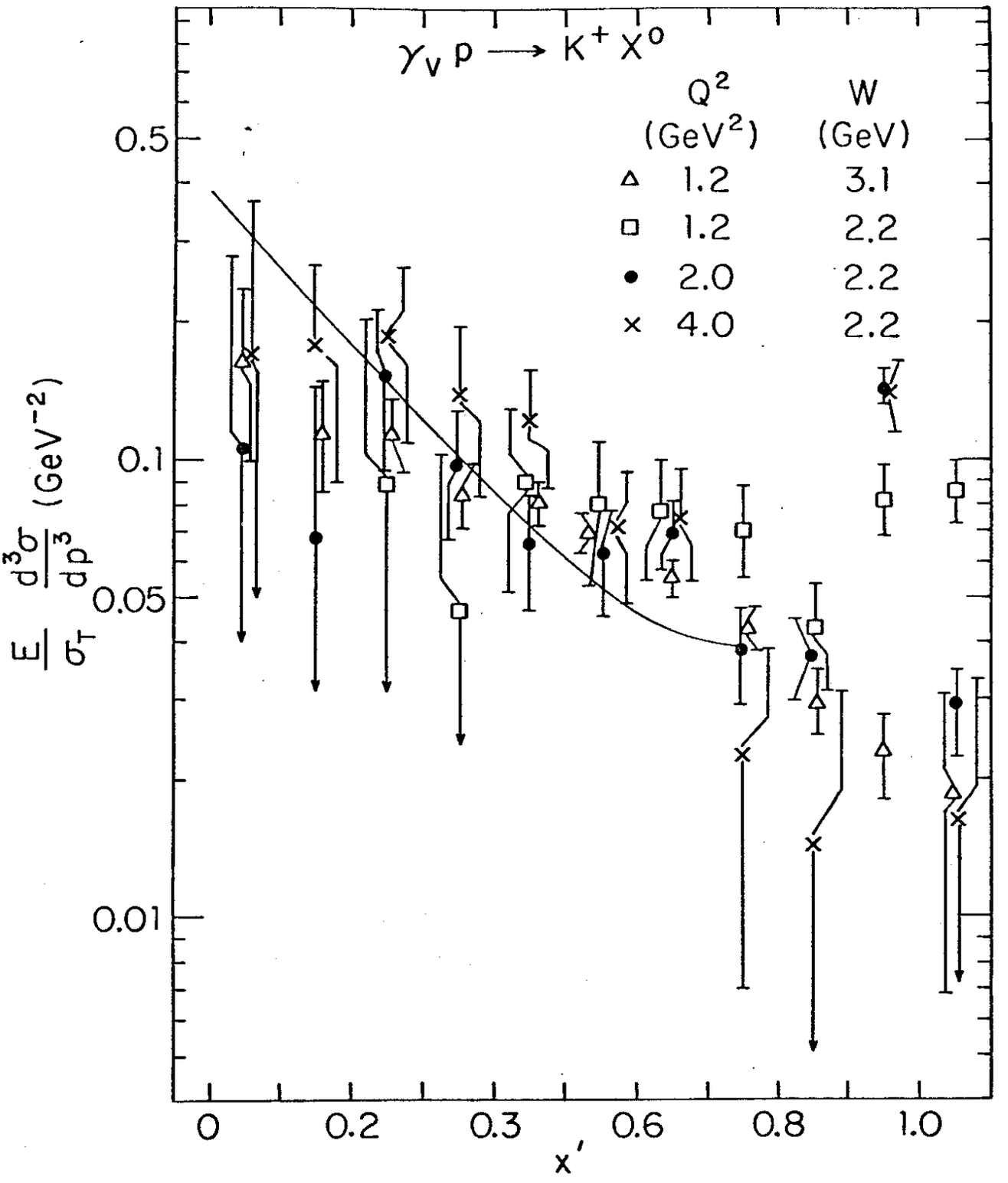
$\gamma_V p \longrightarrow K^+ X^o$
Q^2 (GeV^2)
W (GeV)
1.2 3.1
1.2 2.2
2.0 2.2
4.0 2.2
$\frac{E}{\sigma_T}\frac{d^3\sigma}{dp^3}$ (GeV^{-2})
0.5
0.1
0.05
0.01
0
0.2
0.3
0.6
0.8
1.0
x'

Figure 18

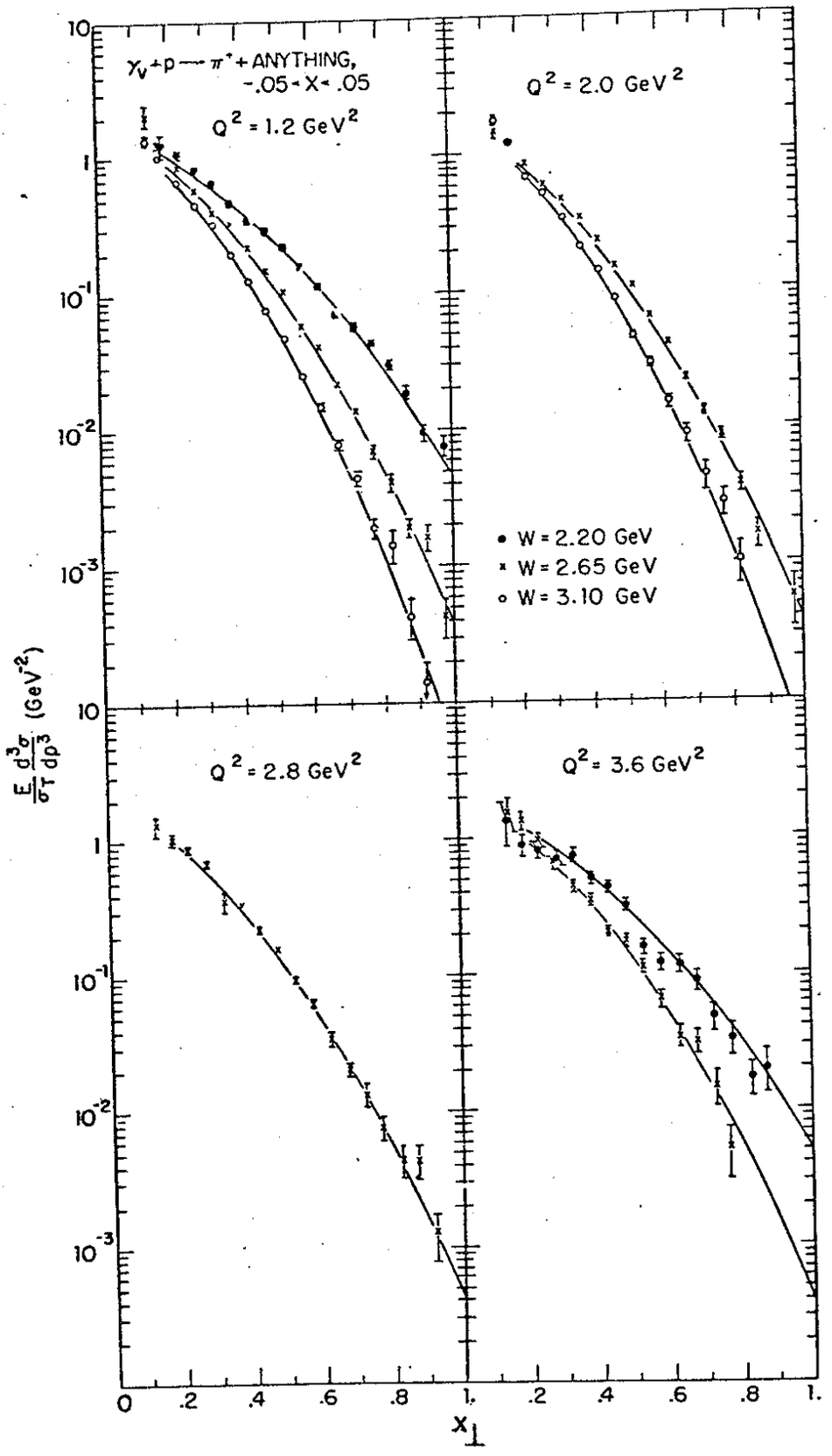
$\gamma_v + p \rightarrow \pi^+ + \text{ANYTHING}$,
$-.05 < X < .05$
$Q^2 = 1.2\ \text{GeV}^2$
$Q^2 = 2.0\ \text{GeV}^2$
$Q^2 = 2.8\ \text{GeV}^2$
$Q^2 = 3.6\ \text{GeV}^2$
• W = 2.20 GeV
× W = 2.65 GeV
○ W = 3.10 GeV
$\frac{E}{\sigma_T}\frac{d^3\sigma}{dp^3}$ (GeV^{-2})
$X_\perp$

Fig. 19

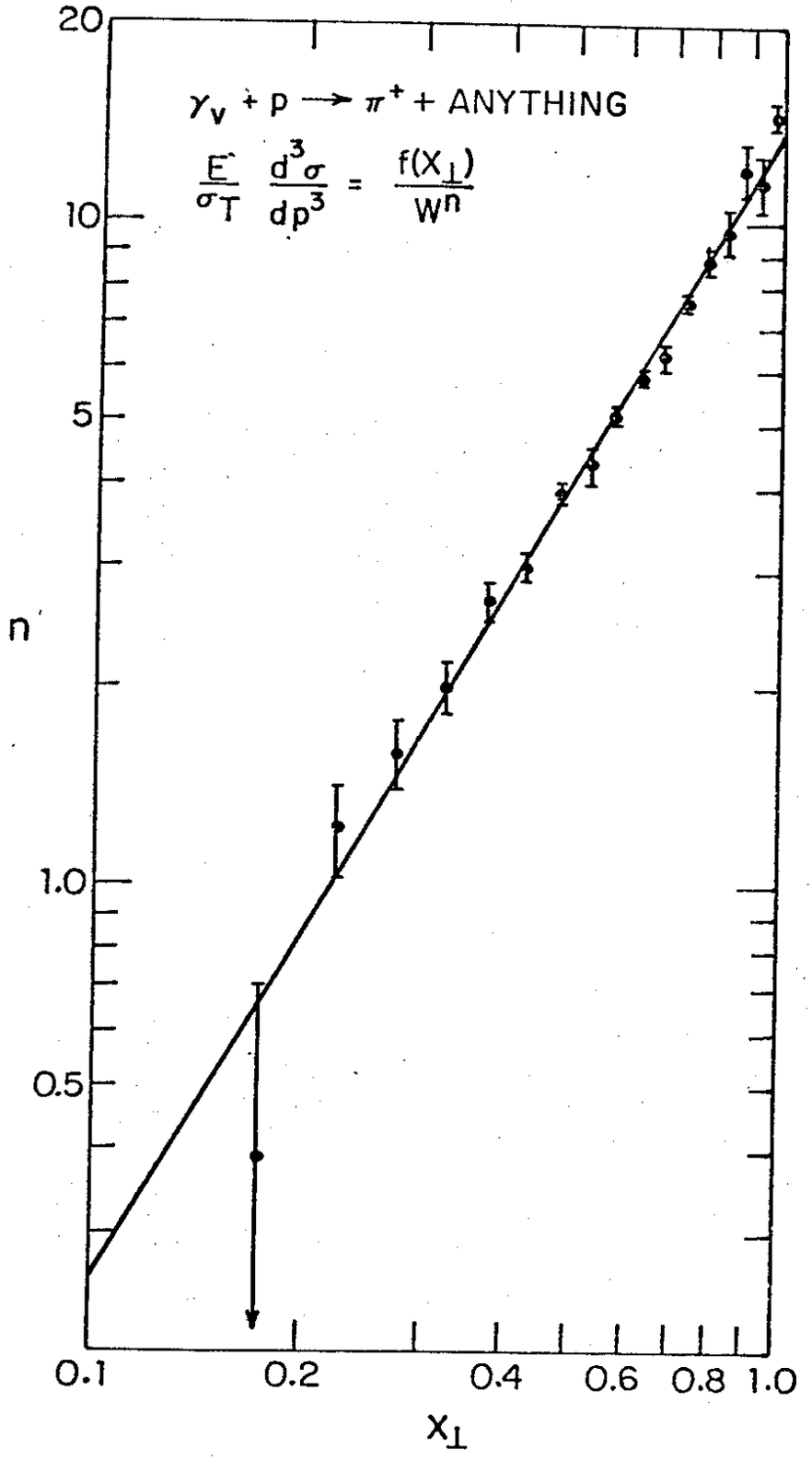
$\gamma_v + p \rightarrow \pi^+ + \text{ANYTHING}$
$\frac{E}{\sigma_T}\frac{d^3\sigma}{dp^3} = \frac{f(X_\perp)}{W^n}$
20
10
5
1.0
0.5
n
0.1
0.2
0.4
0.6
0.8
1.0
$X_\perp$

Figure 20

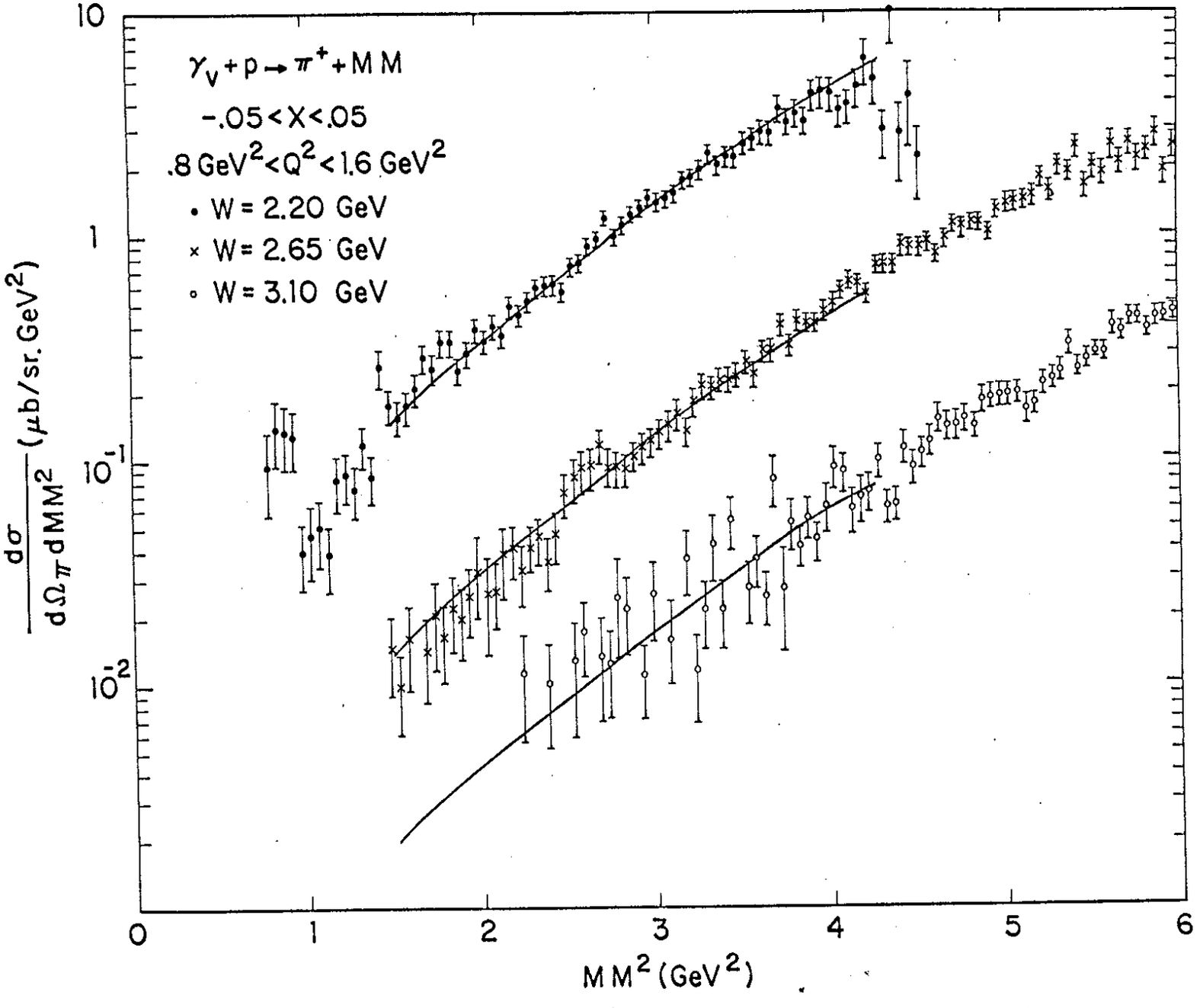
$\gamma_V + p \rightarrow \pi^+ + MM$
$-.05 < X < .05$
$.8\ GeV^2 < Q^2 < 1.6\ GeV^2$
• W = 2.20 GeV
× W = 2.65 GeV
∘ W = 3.10 GeV
$\frac{d\sigma}{d\Omega_\pi dMM^2}$ (μb/sr. GeV^2)
10
1
10^{-1}
10^{-2}
0
1
2
3
4
5
6
MM^2 (GeV^2)

Figure 21

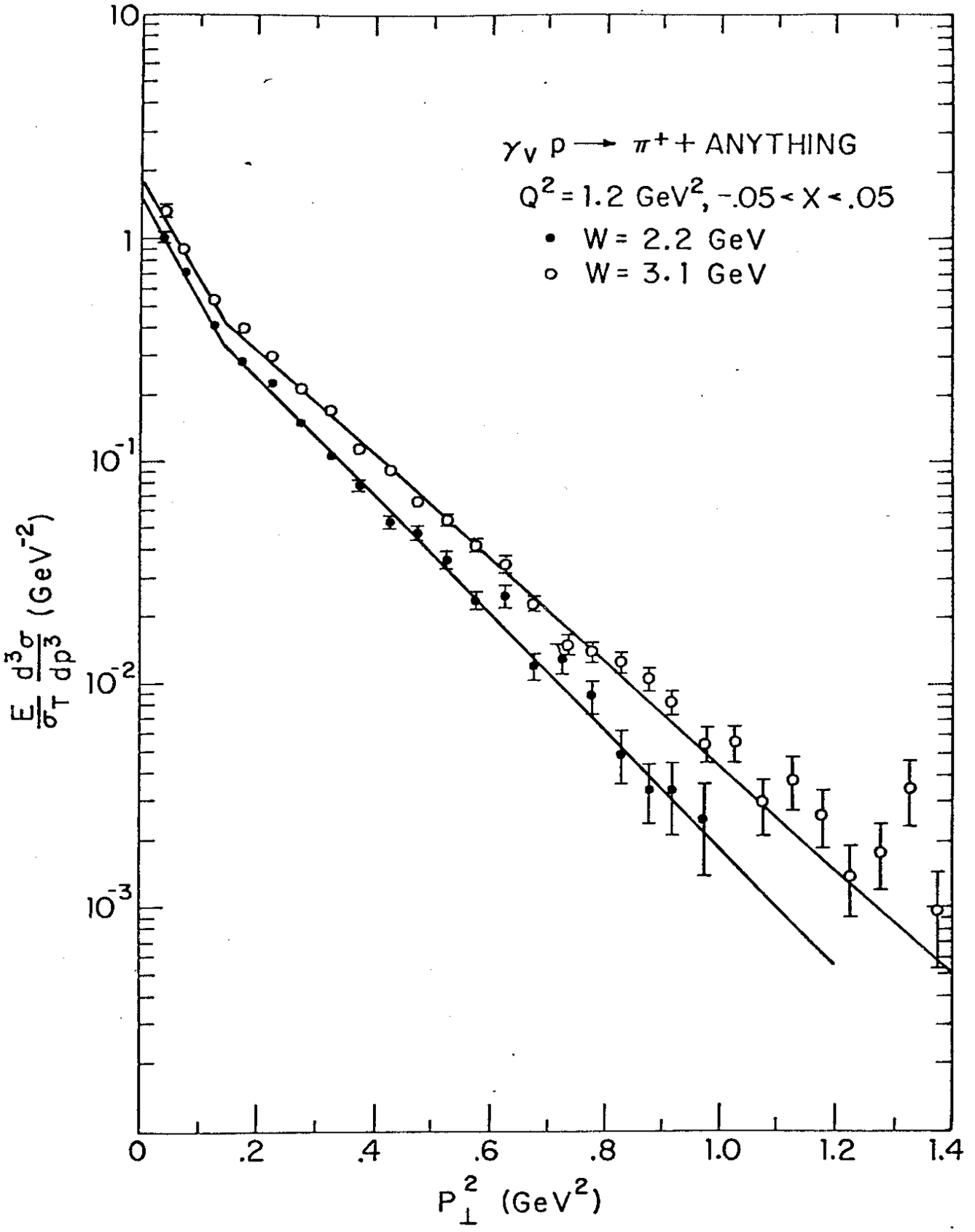
$\gamma_V p \rightarrow \pi^+ + \text{ANYTHING}$
$Q^2 = 1.2\ \text{GeV}^2, -.05 < X < .05$
• W = 2.2 GeV
○ W = 3.1 GeV
$\frac{E}{\sigma_T}\frac{d^3\sigma}{dp^3}$ (GeV^{-2})
$P_\perp^2$ (GeV^2)
10
1
10^{-1}
10^{-2}
10^{-3}
0
.2
.4
.6
.8
1.0
1.2
1.4

Figure 22

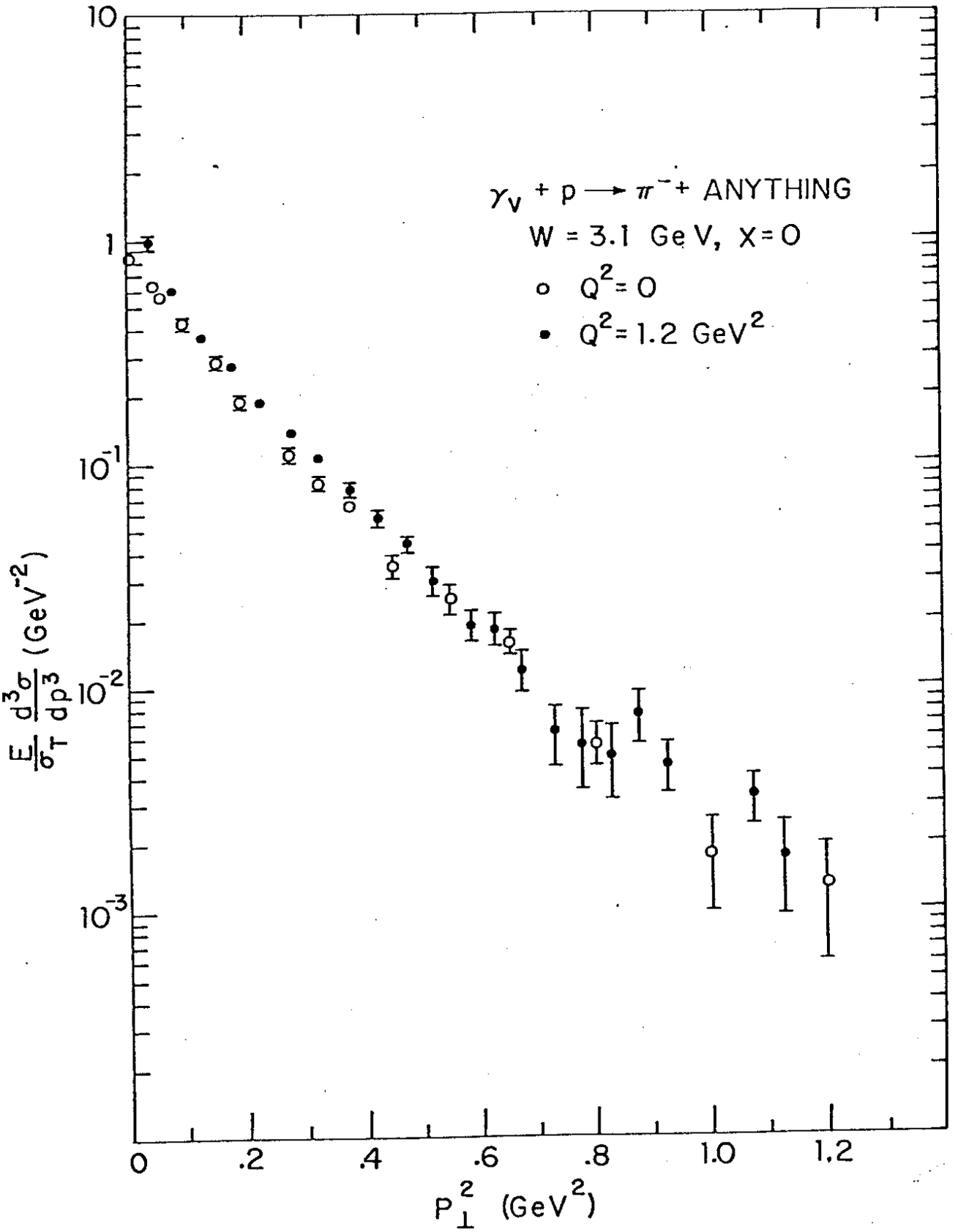
$\gamma_V + p \rightarrow \pi^- +$ ANYTHING
W = 3.1 GeV, X = 0
o $Q^2 = 0$
• $Q^2 = 1.2$ GeV^2
$\frac{E}{\sigma_T}\frac{d^3\sigma}{dp^3}$ (GeV^{-2})
$P_\perp^2$ (GeV^2)
10
1
10^{-1}
10^{-2}
10^{-3}
0
.2
.4
.6
.8
1.0
1.2

Figure 23

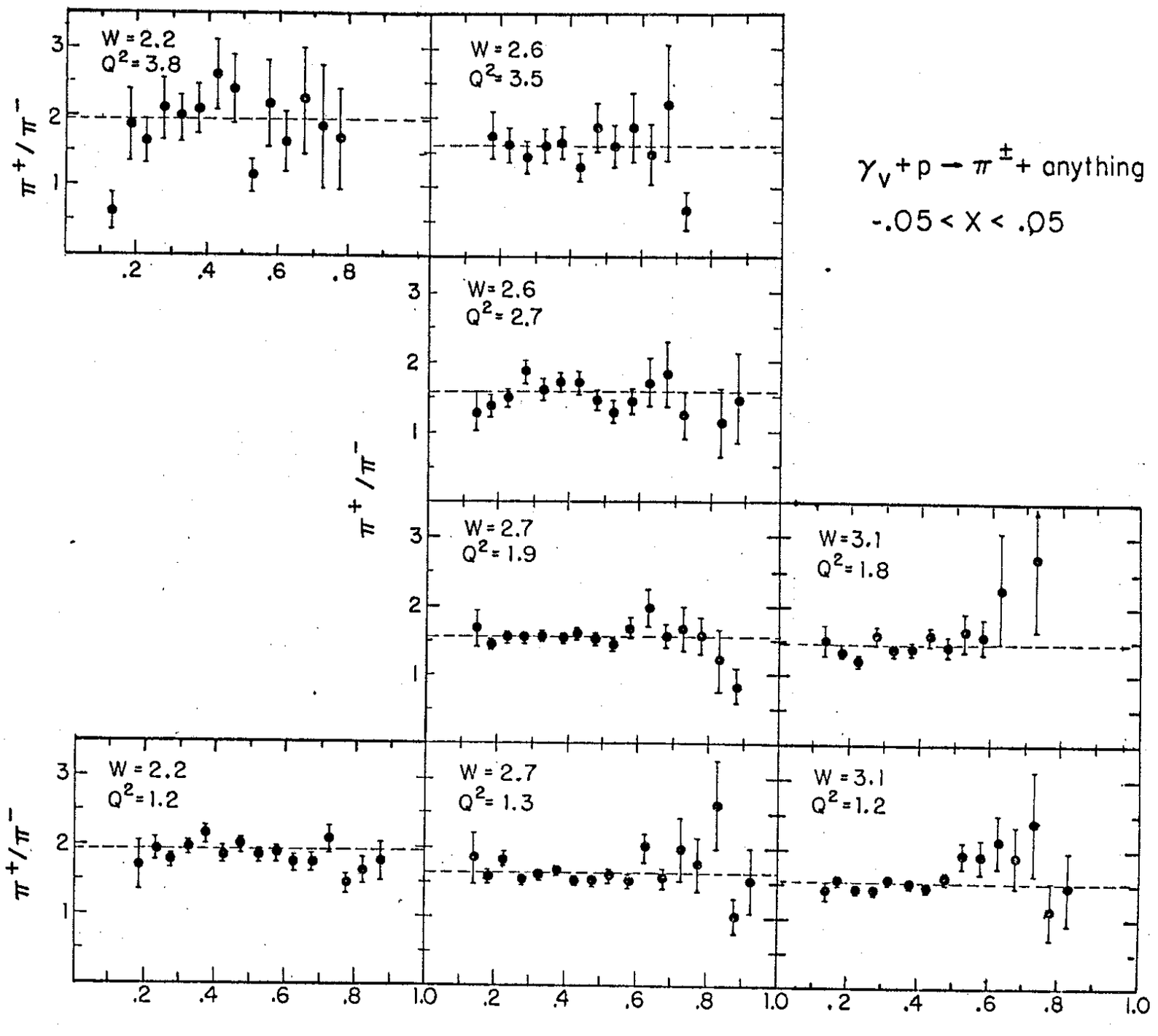

Figure 24

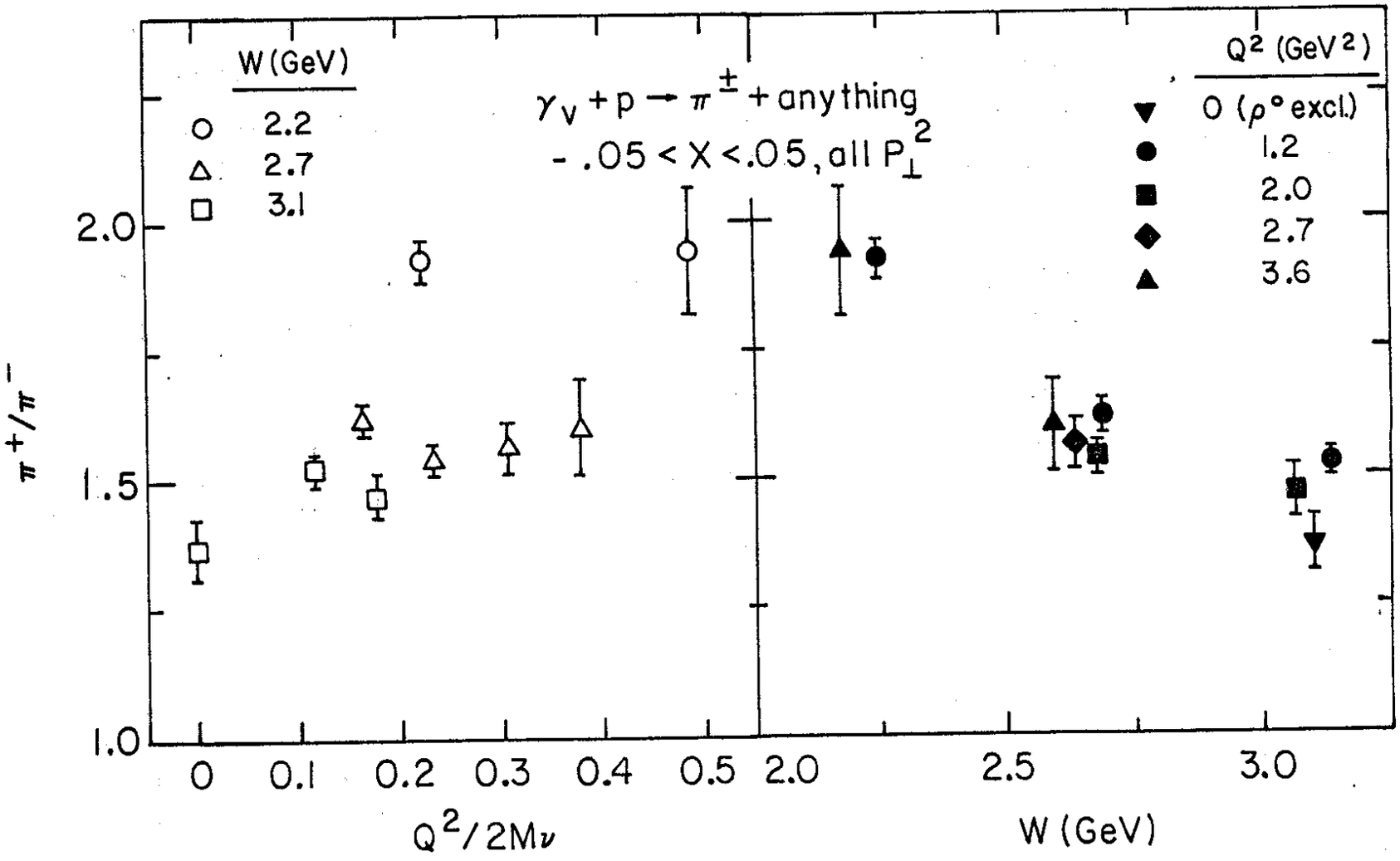
W(GeV)
2.2
2.7
3.1
$\gamma_V + p \rightarrow \pi^{\pm} +$ anything
$-.05 < X < .05$, all $P_\perp^2$
Q^2 (GeV^2)
0 (ρ° excl.)
1.2
2.0
2.7
3.6
π^+/π^-
2.0
1.5
1.0
0
0.1
0.2
0.3
0.4
0.5
2.0
2.5
3.0
$Q^2/2M\nu$
W (GeV)

Figure 25

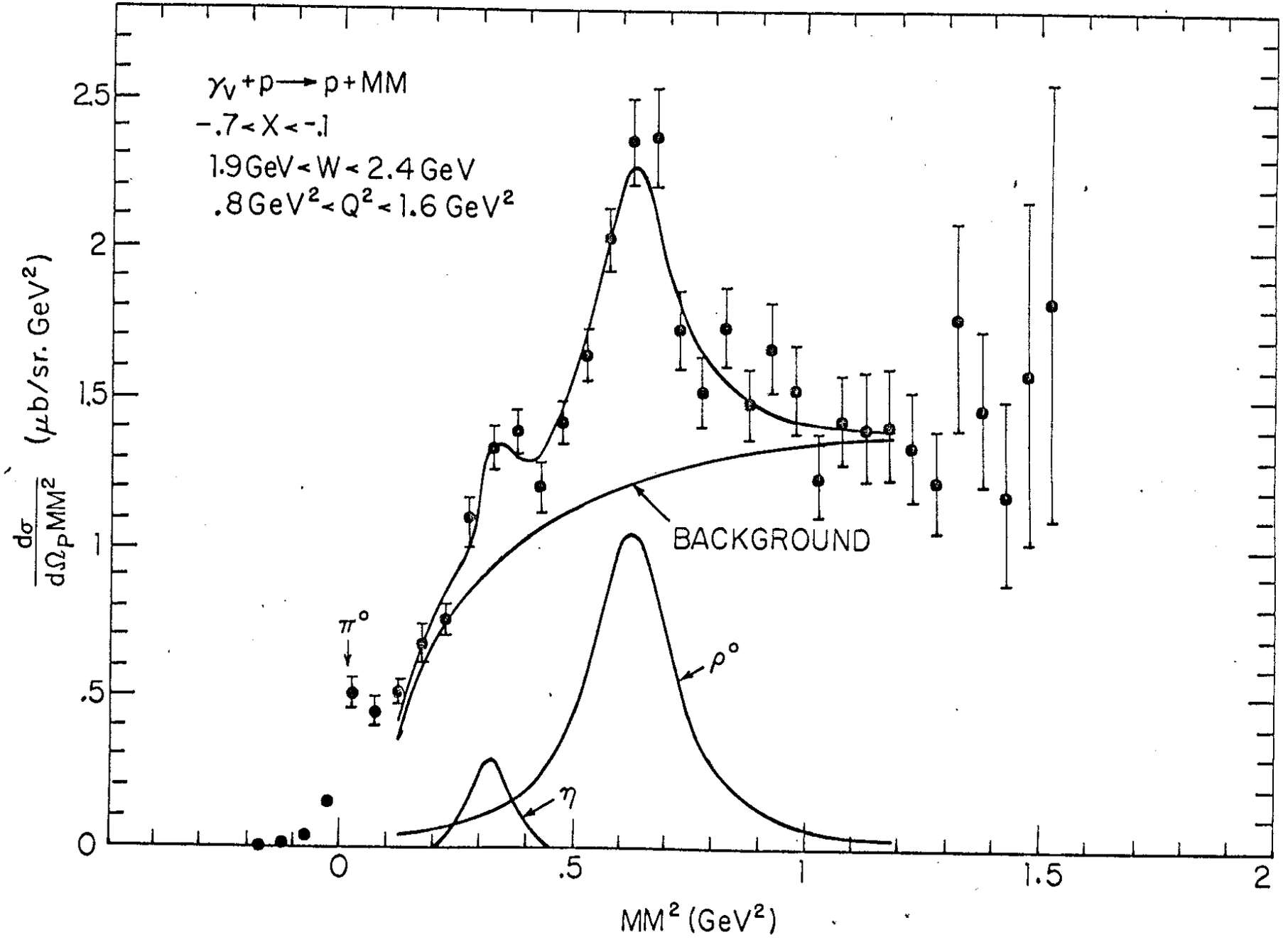

Figure 26

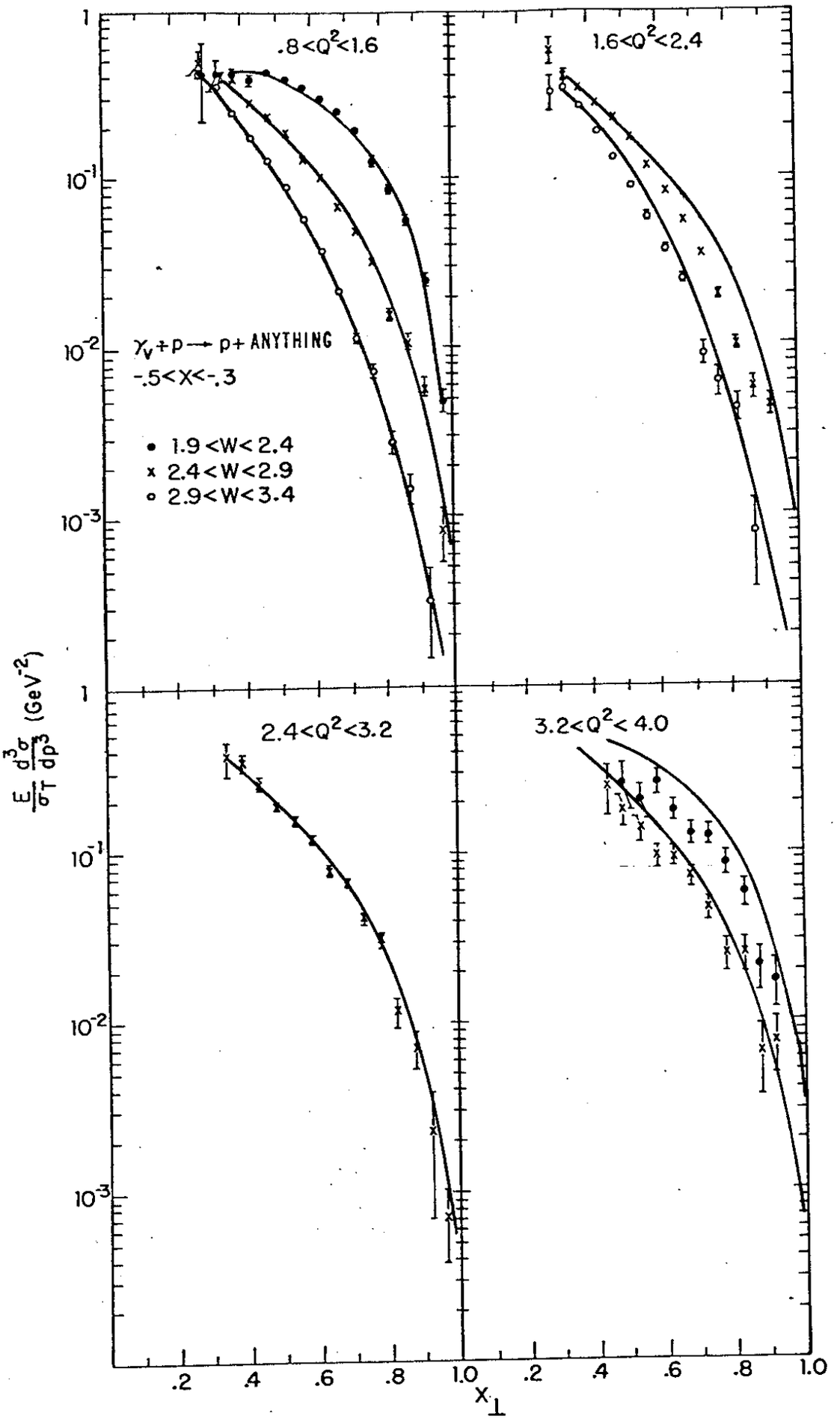
.8<Q²<1.6
1.6<Q²<2.4
2.4<Q²<3.2
3.2<Q²< 4.0
γV+p → p+ ANYTHING
-.5<X<-.3
• 1.9<W<2.4
× 2.4<W<2.9
○ 2.9<W<3.4
E/σT d³σ/dp³ (GeV⁻²)
X⊥
1
10⁻¹
10⁻²
10⁻³
.2
.4
.6
.8
1.0

Figure 27

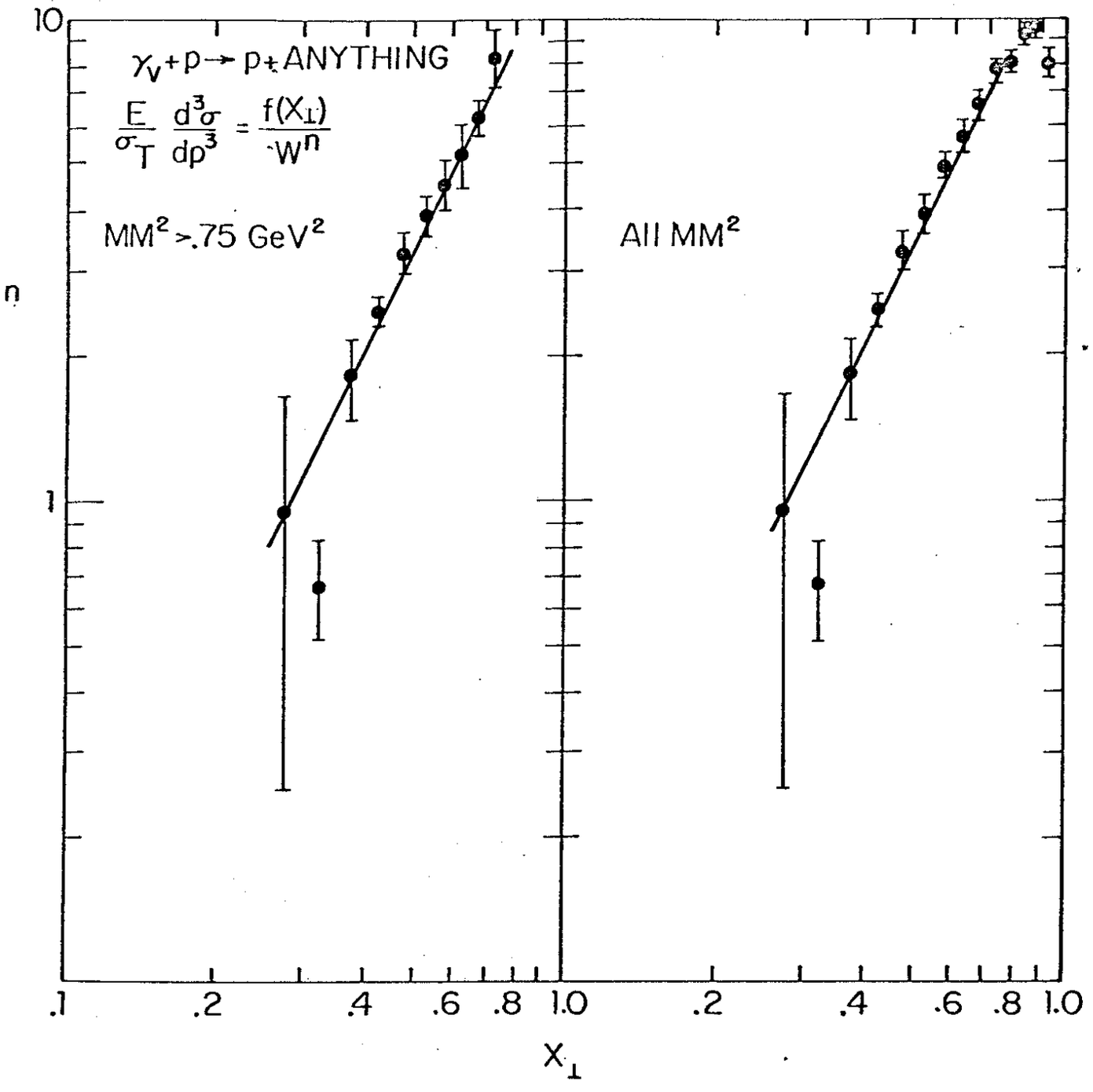

Figure 28

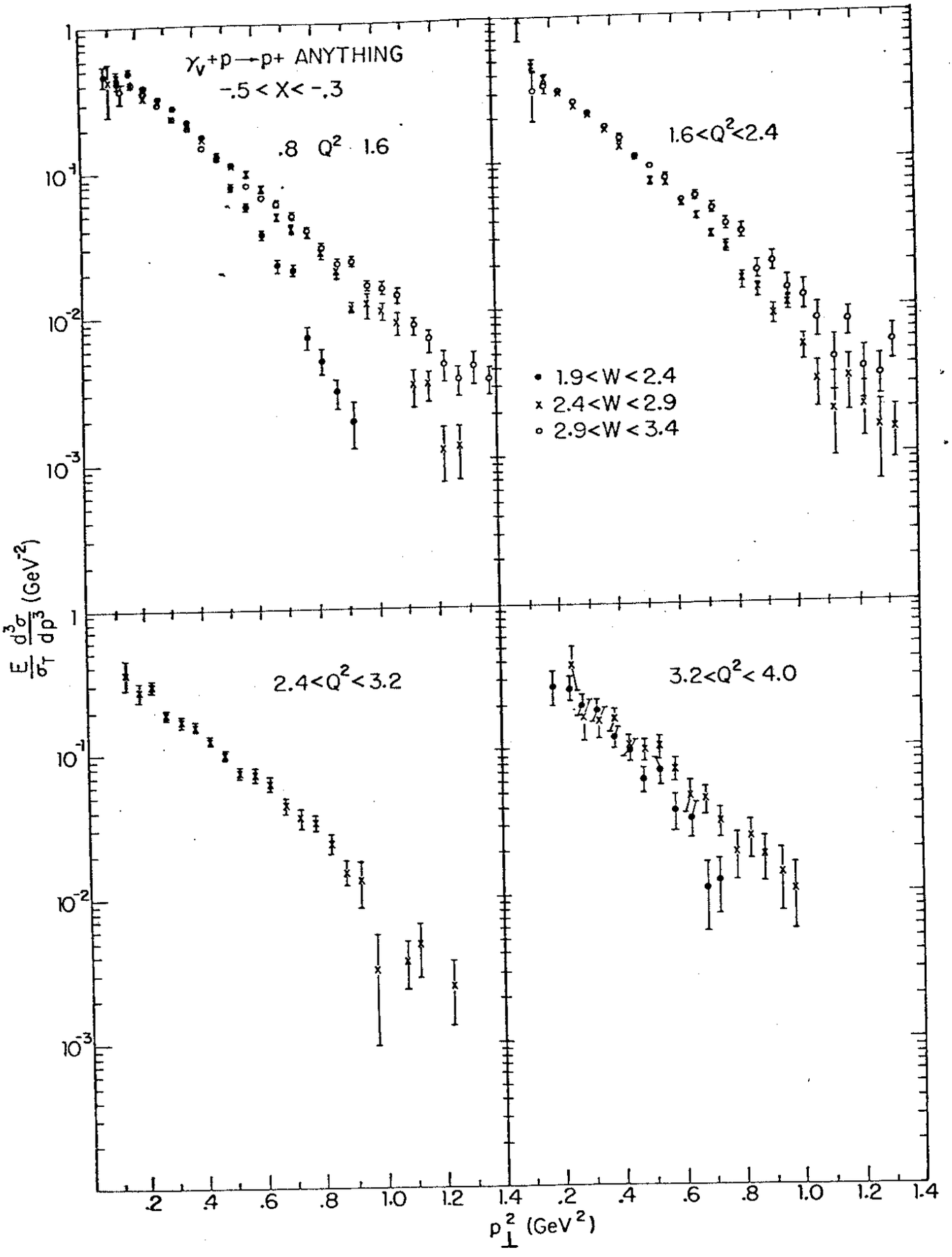

Figure 29

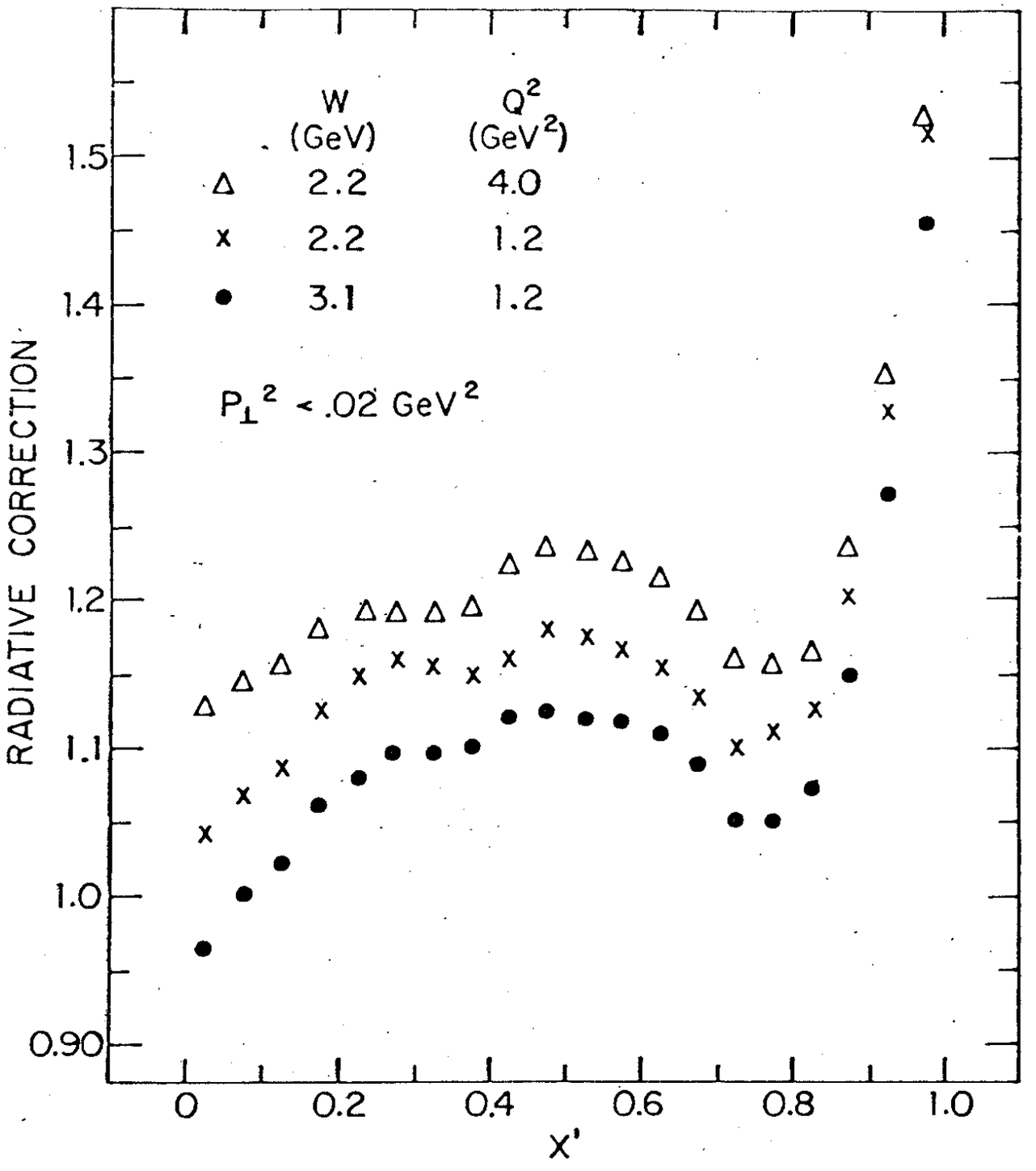
W (GeV)
Q^2 (GeV^2)
2.2 4.0
2.2 1.2
3.1 1.2
$P_\perp^2 < .02\ GeV^2$
RADIATIVE CORRECTION
1.5
1.4
1.3
1.2
1.1
1.0
0.90
0
0.2
0.4
0.6
0.8
1.0
X'

Figure 30

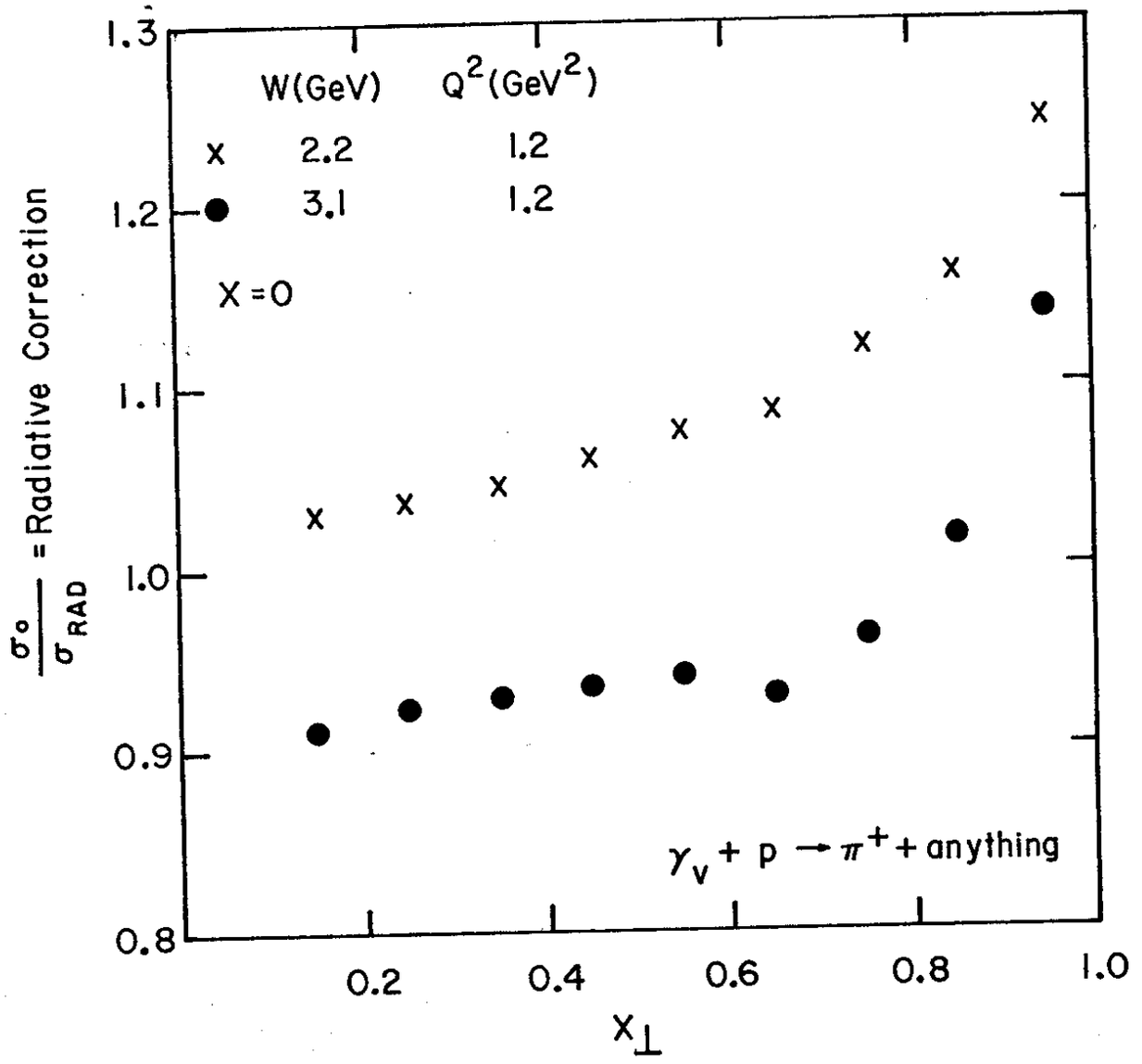

Figure 31

0980875